LEVEL II

12

VSC-TR-81-5

SEMIANNUAL TECHNICAL SUMMARY SEISMIC RESEARCH

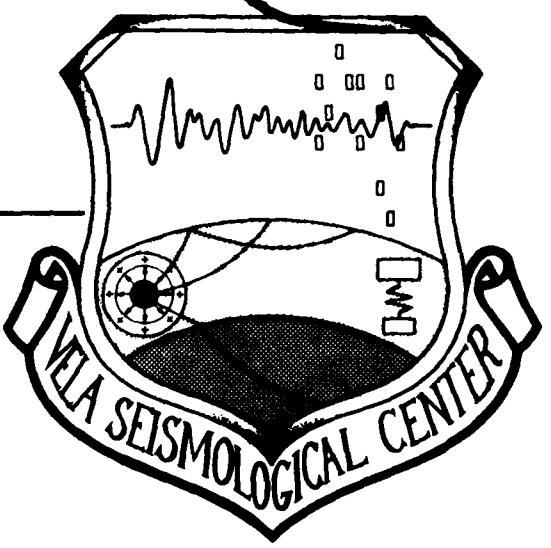

Research Staff - Teledyne Geotech, Alexandria Laboratories
Seismic Data Analysis Center
Teledyne Geotech
314 Montgomery Street
Alexandria Virginia 22314

28 APRIL 1981

Monitored By:
VELA Seismological Center
312 Montgomery Street
Alexandria, VA 22314

Sponsored by

The Defense Advanced Research Projects Agency (DARPA)

DARPA Order No. 2551

(9) Semiannual technical summary.

Unclassified

SECURITY CLASSIFICATION OF THIS PAGE (When Data Entered)

(19) REPORT DOCUMENTATION PAGE	READ INSTRUCTIONS BEFORE COMPLETING FORM
(18) 1. REPORT NUMBER: VSC-TR-81-5	2. GOVT ACCESSION NO.: AD-A098 756
4. TITLE (and Subtitle): SEMIANNUAL TECHNICAL SUMMARY - SEISMIC RESEARCH (6)	5. TYPE OF REPORT & PERIOD COVERED: Technical
	6. PERFORMING ORG. REPORT NUMBER: (14) SDAC-TR-80-5
7. AUTHOR(s): Research Staff - Teledyne Geotech, Alexandria Laboratories	8. CONTRACT OR GRANT NUMBER(s): (15) F08606-79-C-0007, ARPA Order-2,355
9. PERFORMING ORGANIZATION NAME AND ADDRESS: Teledyne Geotech, 314 Montgomery Street, Alexandria, Virginia 22314 (408258)	10. PROGRAM ELEMENT, PROJECT, TASK AREA & WORK UNIT NUMBERS: T/0709/B/PMP
11. CONTROLLING OFFICE NAME AND ADDRESS: VELA Seismological Center, 312 Montgomery Street, Alexandria, Virginia 22314 (11)	12. REPORT DATE: May 80
	13. NUMBER OF PAGES: 70 (12) 72
14. MONITORING AGENCY NAME & ADDRESS (if different from Controlling Office): Defense Advanced Research Projects Agency, 1400 Wilson Boulevard, Arlington, Virginia 22209	15. SECURITY CLASS. (of this report): Unclassified
	15a. DECLASSIFICATION/DOWNGRADING SCHEDULE

16. DISTRIBUTION STATEMENT (of this Report)

APPROVED FOR PUBLIC RELEASE; DISTRIBUTION UNLIMITED.

17. DISTRIBUTION STATEMENT (of the abstract entered in Block 20, if different from Report)

18. SUPPLEMENTARY NOTES

19. KEY WORDS (Continue on reverse side if necessary and identify by block number)

Crust effects
L_g, P_n, P_g
SALMON
Detection
Location
pP
Reduced Displacement Potential

20. ABSTRACT (Continue on reverse side if necessary and identify by block number)

This report summarizes the main results of the research work at SDAC on contract F08606-79-C-0007, obtained within the time period October 1979-March 1980. This report is not meant to give details of the work performed. The same results will be presented in detail in separate topical reports on all the major projects given here.

DD FORM 1 JAN 73 1473 EDITION OF 1 NOV 65 IS OBSOLETE

Unclassified 408258

SECURITY CLASSIFICATION OF THIS PAGE (When Data Entered)

SEMIANNUAL TECHNICAL SUMMARY - SEISMIC RESEARCH

SEISMIC DATA ANALYSIS CENTER REPORT NO.: SDAC-TR-80-5

AFTAC Project Authorization No.:	VELA T/0709/B/PMP
Project Title:	Seismic Data Analysis Center
ARPA Order No.:	2551
Name of Contractor:	TELEDYNE GEOTECH
Contract No.:	F08606-79-C-0007
Date of Contract:	01 October 1979
Amount of Contract:	$689,760
Contract Expiration Date:	30 September 1980
Project Manager:	Robert R. Blandford (703) 836-3882

P. O. Box 334, Alexandria, Virginia 22314

APPROVED FOR PUBLIC RELEASE; DISTRIBUTION UNLIMITED.

ABSTRACT

This report summarizes the main results of the research work at SDAC on contract F08606-79-C-0007, obtained within the time period October 1979-March 1980. This report is not meant to give details of the work performed. The same results will be presented in detail in separate topical reports on all the major projects given here.

TABLE OF CONTENTS

LIST OF FIGURES

LIST OF FIGURES (Con't)

LIST OF FIGURES (Con't)

LIST OF TABLES

PROPAGATION IN SHIELDS

A. Effect of Crustal Structure

A basic understanding of the mechanisms of propagation and the generation of regional phases is necessary for improving location, yield estimation and discrimination using regional phases. Due to the multi-modal structure of such signals, mode theory in layered media needs to be used.

Ever since the identification by Press and Ewing (1952) of the short-period surface wave L_g as a distinct seismic phase (or, more properly, a sequence of phases), an effort has been concentrated on understanding its origin and the effects of earth structure on its propagation and attenuation. In particular, it was necessary to explain why L_g was apparently unable to travel through even small segments of oceanic lithosphere and to determine whether, as it was sometimes conjectured, L_g was a channel wave whose occurrence indicated the existence of a high-velocity lid trapping energy in a low-velocity zone (LVZ). A major step towards understanding the nature of L_g was taken by Oliver and Ewing (1957), who noted that the group velocities of prominent maxima in the L_g wavetrain correspond to those of higher-mode Love waves. This identification of L_g as a superposition of short-period higher-mode Love waves was reinforced convincingly by Knopoff et al (1973), who demonstrated by means of synthetic seismograms that realistic seismic source mechanisms and earth structures could produce higher-mode Love waves of sufficient amplitude at the proper frequencies to account for the observations of L_g, at least to first order.

We have undertaken to expand upon the modal superposition technique in order to answer some questions about L_g propagation which ought to be understood if L_g is to be used in a program of seismic discrimination at regional distances. In particular, it is well known that L_g not only fails to propagate through the ocean but also attenuates rapidly in certain continental regions. It is also known that the amplitude of L_g, as well as its group velocity, is strongly influenced by surficial geology. In order to interpret observations of L_g in terms of the source mechanism, as well as to choose the best sites for locating future seismic stations, it is important to have a quantitative estimate of these path effects. We should also like to know, for a given source-to-receiver earth model, how large a variability in the characteristics of L_g can be anticipated from earthquakes of different source

mechanisms and of different depths. It is especially important to know whether certain earthquakes have some L_g signal characteristics which can be used as diagnostics in discrimination studies. Our study of L_g synthetic seismograms has been aimed at investigating these questions.

In order to produce the synthetic seismograms by modal superposition, it is necessary first to assume a flat, plane-parallel earth model and to calculate the dispersion relation (i.e., phase velocity as a function of frequency) for every Love-wave mode of this model. The results of a typical calculation are shown in the accompanying Figure 1. The high-velocity cut-off is the shear-wave velocity at the Moho, since higher velocities correspond not to L_g but to the mantle channel wave S_n (Stephens and Isacks, 1977). In the interest of computational efficiency, synthetics were sampled at five points per second, and thus no frequencies greater than the folding frequency of 2.5 Hz were considered; this cut-off results in the inclusion of twenty-six Love-wave modes for this particular earth model (Canadian shield with no surficial sediments). It is important to note the strong curvature in the graphs of the individual modes at certain frequencies; for earth models with velocity contrasts greater than those in a shield model, a curvature can be very strong and, for models with a crustal LVZ, the modes osculate. Because the group velocity curves are related by differentiation to the phase velocity curves, it is necessary that the phase velocity curves be approximated accurately in the regions of strong curvature or else the synthetics will be marred by spurious arrival times, a problem noted by Helmberger and Harkrider (1980). In order to lessen the effects of this problem we have recently revised our program to utilize a four-point Lagrangian interpolation for the phase velocity at those discrete Fourier frequencies used in the synthesis. Also shown are the particle displacements as a function of depth for certain modes at a particular frequency in Figure 2. It is seen that most of the energy in the fundamental mode is confined to the top few kilometers of the crust, a phenomenon which will be important in considering the effect of a surficial layer of low-velocity sediments. For certain frequencies and certain modes, the displacement (and the tangential stress) eigenfunctions are not well behaved in the bottom layer of propagation above the attenuating half-space. This behavior is due to computational inaccuracy in the cumulative multiplication of layer matrices, a phenomenon well known to all investigators in this field. Finally, there is shown an example of the superposition of the twenty-six Love-wave modes to produce L_g in Figure 3.

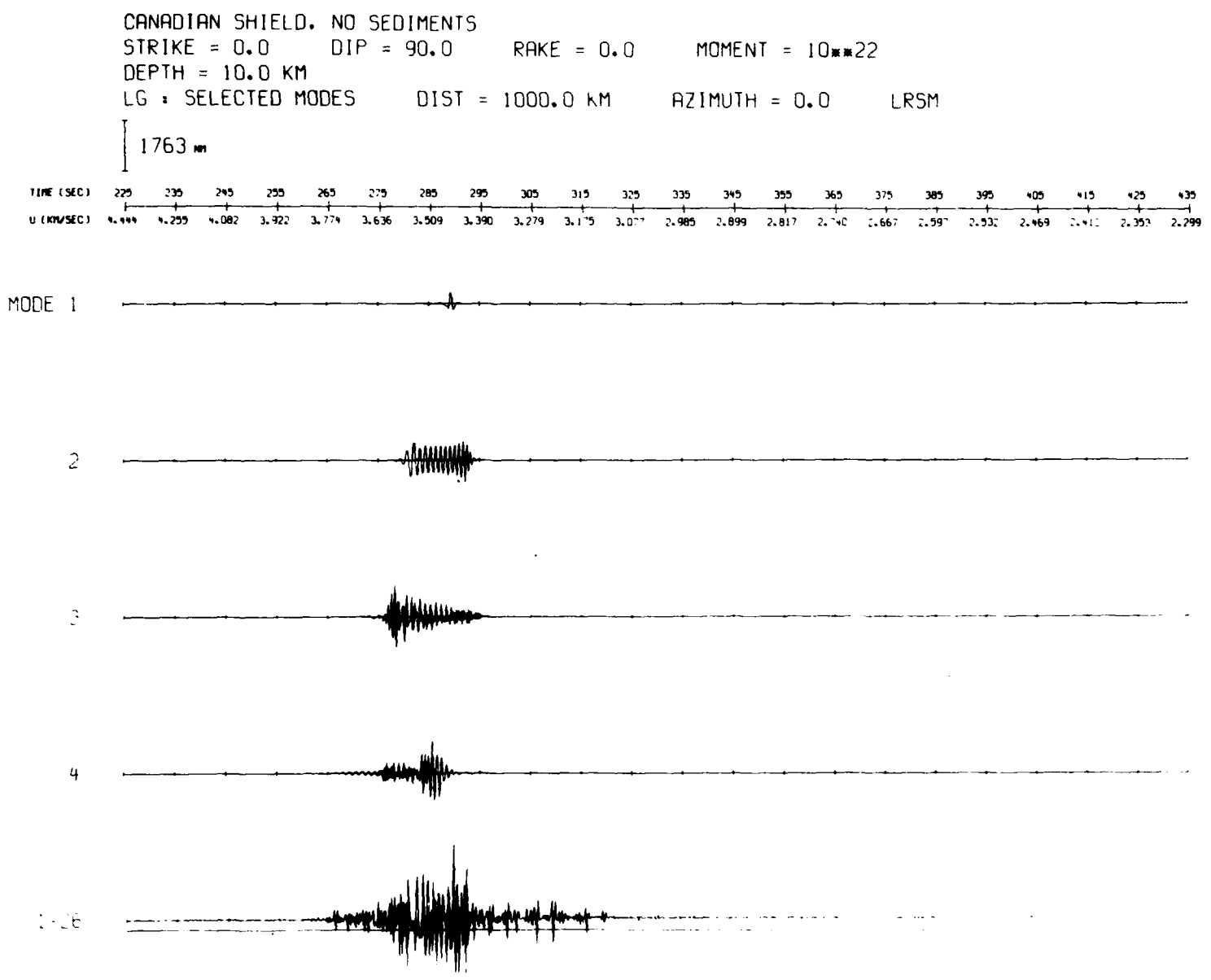

Figure 1. Synthesis of L_g for a particular double-couple mechanism and a particular source-to-receiver distance. The first four modes are shown separately along with the superposition of all twenty-six modes. The early-arriving energy, discussed in the text, is due to the error in the phase velocities resulting from linear interpolation of the dispersion relation curves.

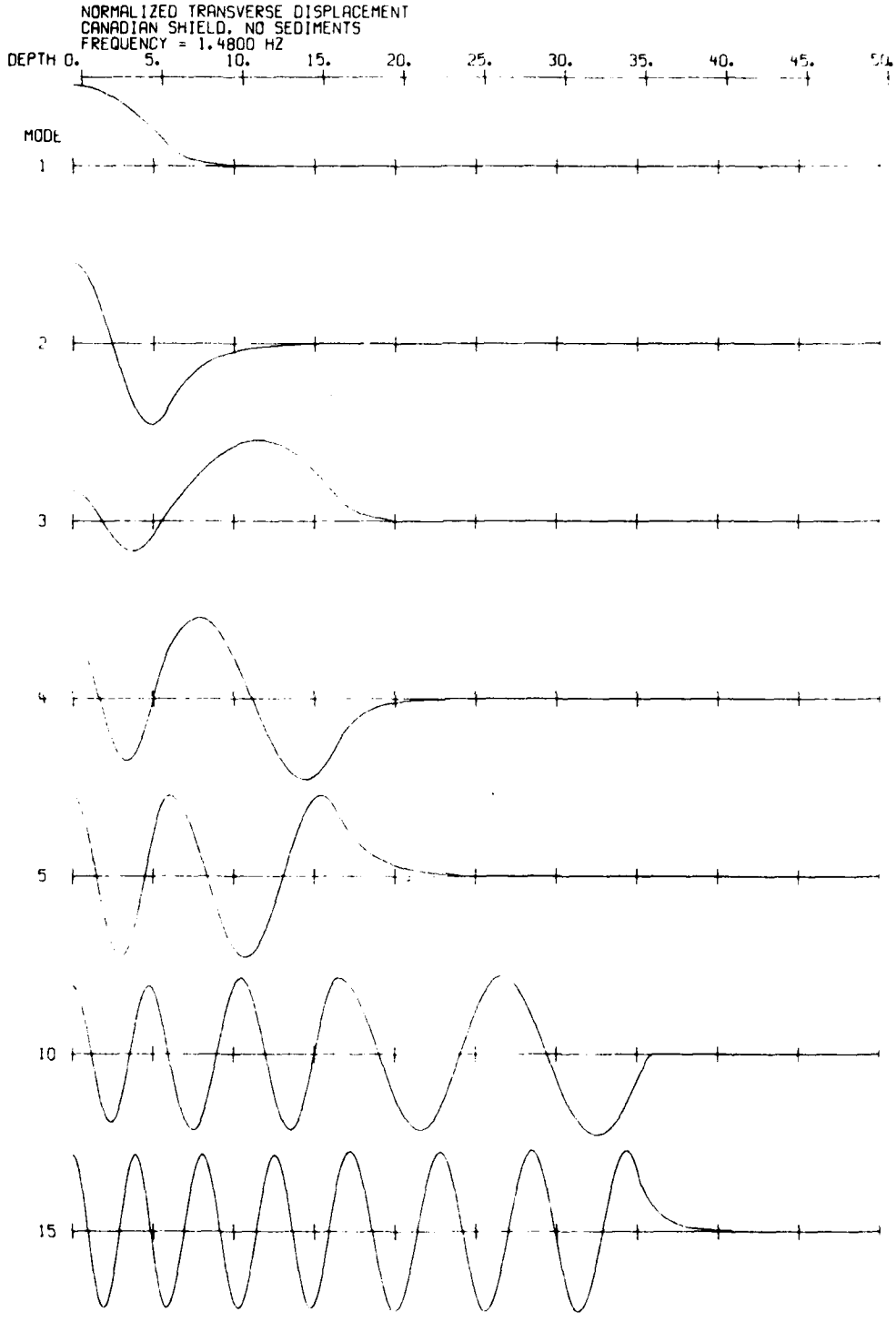

Figure 2. Particle displacement (normalized to the surface displacement) as a function of depth for seven selected Love-wave modes at a particular frequency.

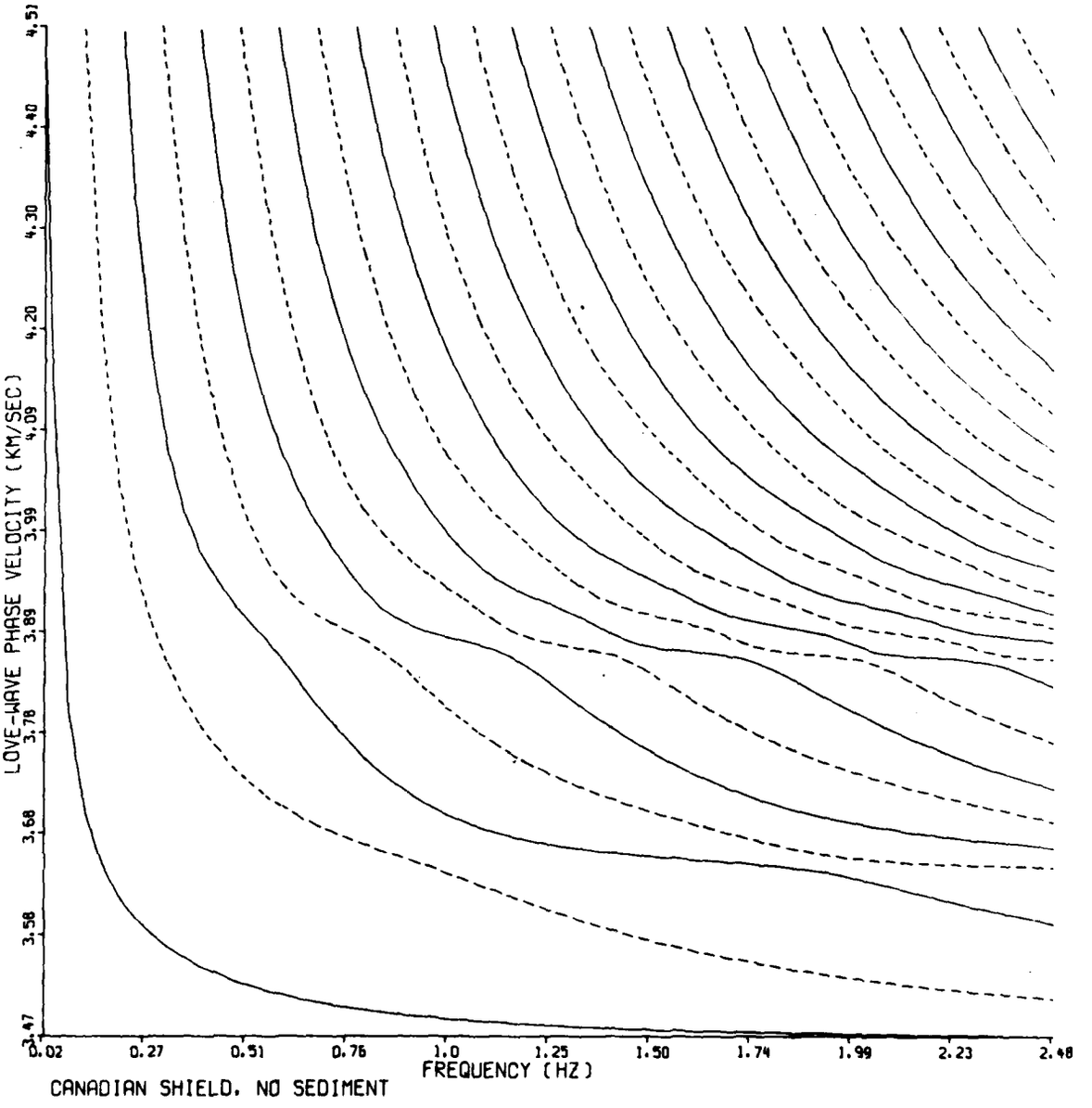

Figure 3. Dispersion relations for 26 Love-wave modes.

Synthetics have been produced for a variety of double-couple source mechanisms located at various depths and observed at various distances. An especially significant case which has been treated is that of a linear array of closely spaced instruments. Such an array is capable of measuring L_g phase velocity by means of frequency-wavenumber processing (Mrazek et al, 1980). Preliminary results indicate that the phase velocity is greater (at a given frequency) for deeper events, since they preferentially excite the higher, faster modes. If a more detailed investigation which is currently underway upholds this result, then L_g would in fact be shown to be a useful discriminant for earthquakes occurring at depths of greater than a few kilometers. Also being examined is the decay of amplitude with distance for path lengths of up to 1800 km. It is important to determine whether this decay is sensitive to the source mechanism, since the surface-wave excitation is highly variable, depending upon the spatial orientation of the double-couple. Not only the amplitude of the L_g wavetrain envelope but also its temporal extent is being compared, at certain distances, with observations. It appears that the modal superposition predicts a wavetrain of shorter duration than is observed. The late-arriving energy in the observed L_g envelopes is probably due to waves which have been scattered by topographic and geologic inhomogeneities (on the scale of an L_g wavelength) and which have undergone conversion to (slower) Rayleigh modes. Energy which is transmitted in the form of Rayleigh modes not only lengthens the coda of L_g but also gives rise to particle displacements in the vertical and radial directions. This phenomenon is currently not modeled by the synthetics.

The Love-wave dispersion and eigenfunction calculations have been completed for a Canadian shield model topped by a 2-km thick sedimentary layer. Synthetics will be run for this second model when analysis is completed of those which have been produced using the hard rock model. Another model is being prepared for which the anelasticity Q is depth-dependent within the crust. This will result in a surface-wave attenuation which is both frequency- and mode-dependent, and it will be important to determine what effect this has upon the amplitude-distance relation and upon the F-K plots which would be measured at various distances. We note that Knopoff et al (1974), examining the mantle LVZ by means of L_g synthesis at longer wave-lengths than we are considering, invokes a depth-dependent Q as the explanation of why L_g fails to propagate in an oceanic earth model.

In order to account for the L_g energy which arrives late in the coda in the form of Rayleigh modes, work is underway to develop a Rayleigh-wave counterpart for the Love-wave modal superposition. To this end, a Rayleigh-wave dispersion program which utilizes the algorithm of Abo-Zena (1979) which is more accurate for high frequencies and higher modes than are the conventional algorithms has been programmed. The numerical difficulties arising in the computation of the kinetic energy integral for the layered halfspace and in the computation, via propagator matrices, of the vertical and radial displacement and stress eigenfunctions remain to be addressed.

D. W. Rivers

B. Site Effects on Regional Phases

Since yield estimation of regional events is based on wave amplitudes, and since envelope shapes may be diagnostic of source depth, the effect of geological structures under the observing sites on these signal properties must be evaluated.

In our previous work at NTS we have shown that at sites underlain by low velocity materials, the amplitudes of the regional phases P_g and L_g were amplified by factors up to 10, and the envelope shapes of both phases also changed, resulting in a prolongation of wavetrains at those sites (Barker et al, 1979). The observed site effect for L_g and P_g appear, therefore, to be several times greater than that for teleseismic P and would seriously affect any yield estimates based on measurements on these phases. The sites at NTS were closely spaced such that differences in paths, as manifested in multipathing, source radiation patterns and varying geophysical properties along the paths, do not seriously affect the conclusions about site effects. To further investigate site effects, we have undertaken the analysis of regional phase amplitudes at LRSM stations located in the north-central region of the US and some adjoining regions of Canada. The stations analyzed thus far are shown in the enclosed map (Figure 4) showing the events used. The event parameters are listed in Table I. Amplitudes of all identifiable regional phases were read at each station. In addition for L_g, the envelope shape was characterized by noting the time of the onset of the phase, the time at the maximum and finally, where the envelope decreased to one-half of the maximum. The L_g amplitudes used in the estimation of site effects were at the maximum of the magnitude.

The L_g amplitudes were corrected to a common distance of 500 km using the Δ^{-2} fall-off rate appropriate to the EUS. The station sites were subdivided into two groups: hardrock sites and sedimentary sites. This subdivision is also indicated in Figure 4. The distance corrected amplitudes were also corrected for event magnitude by dividing them with the average of hardrock site amplitudes. Histograms of these reduced amplitudes of L_g for two types of sites (Figure 5), clearly show the effect of site amplification. The average of the sedimentary site amplitudes is larger by a factor of 1.34 (about .13 amplitude units). This contrast is considerably less than at NTS. This is explainable by the fact that the sedimentary sites we examined do not have the thick, extremely low-velocity sediments or volcanics present at Pahute Mesa and Yucca Flats, and many sedimentary sites are actually on fairly well consolidated rocks. The P_n amplitudes

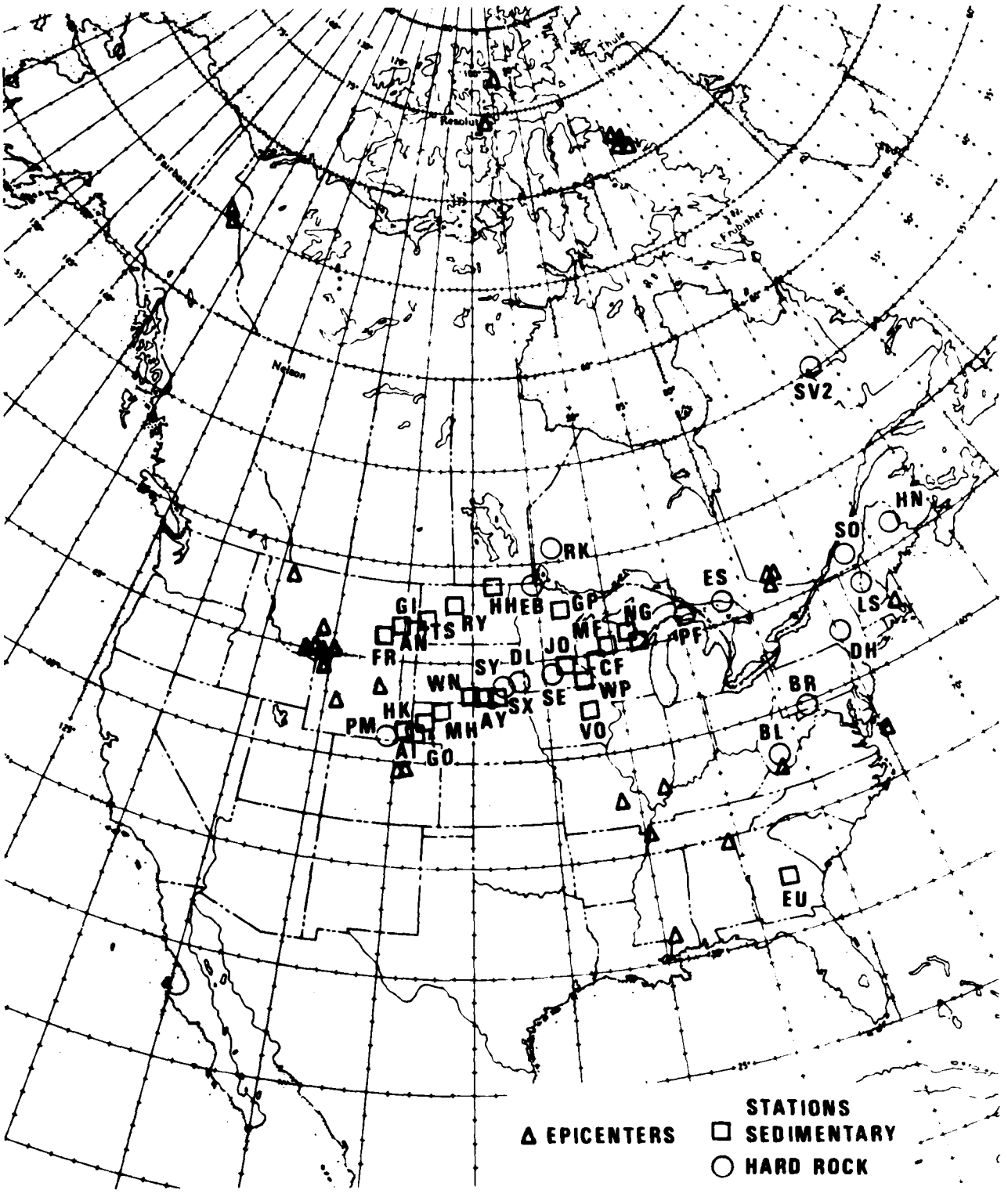

Figure 4. Map of events and LRSM stations used for the study of site effects.

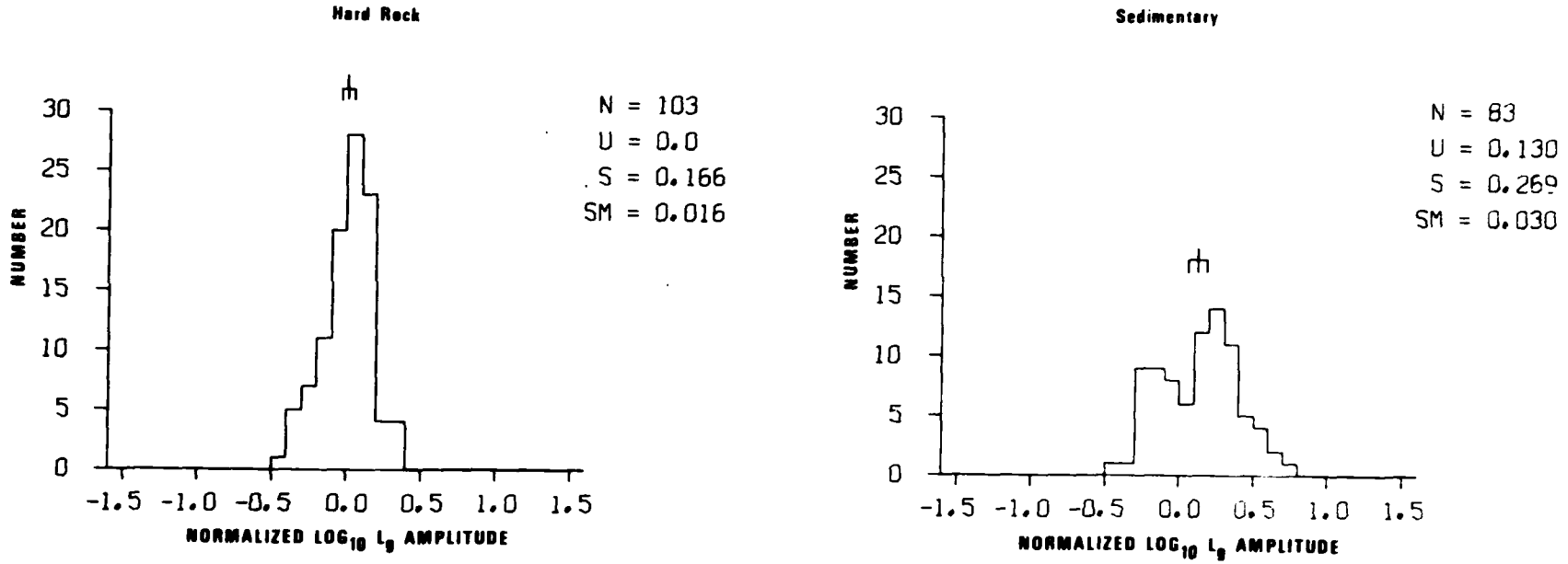

Figure 5. Histogram of the distance and magnitude corrected L_g amplitudes at hard rock (left) and sedimentary sites. Explanation of symbols U - mean, S - standard deviation, SM - standard deviation of the mean.

TABLE I

Event List For Regional Phase Study

Date	Origin Time	Location	Latitude	Longitude	Magnitude	Depth (km)
15 Jul 62	11 59 21.9	Montana	45.0N	110.2W		25
23 Jul 62	06 05 18.4	New Madrid	36.1N	89.8W		18
22 Oct 62	05 03 03.9	Montana	45.2N	111.3W		33
04 Nov 62	06 18 31.5	Yellowstone	44.3N	110.3W		
04 Dec 62	17 49 59.4	Colorado	39.8N	104.7W		33
28 Dec 62	10 01 23.6	Montana	48.4N	113.9W		33
30 Jan 63	05 05 59.5	Montana	45.0N	110.8W		33
30 Jan 63	23 05 09.6	Colorado	39.8N	104.6W		33
16 Feb 63	03 01 41.0	Montana	46.1N	111.0W		33
25 Feb 63	18 45 16.5	Wyoming	42.6N	109.2W		33
08 Mar 63	00 14 15.6	Q. Eliza. Is.	76.7N	94.9W	3.9	33
20 Jul 63	00 11 35.0	N. Yukon	65.2N	133.7W	4.6	
03 Aug 63	00 37 50.3	S. Illinois	37.0N	88.8W		18
04 Sep 63	21 20 18.5	Baffin Is.	71.5N	72.8W	4.1	33
04 Sep 63	21 41 00.6	Baffin Is.	71.6N	73.5W	4.4	33
06 Sep 63	01 46 13.0	Baffin Is.	71.5N	73.0W	4.4	33
12 Oct 63	02 46 48.1	Baffin Is.	71.6N	73.0W	4.1	33
15 Oct 63	12 28 58.4	S. Quebec	46.6N	77.6W		18
15 Oct 63	13 59 49.7	S. Quebec	46.3N	77.8W	3.8	14
16 Oct 63	15 31 01.8	S. New Eng.	42.5N	70.8W		20
08 Jan 64	10 04 31.6	S. Quebec	46.1N	77.7W	3.8	33
18 Feb 64	09 31 10.5	Alabama	34.8N	85.5W		15
18 May 64	01 04 30.5	N. Eliza. Is.	74.3N	97.4W	4.1	15
27 Aug 64	09 53 51.1	N. Yukon	65.3N	133.8W	4.6	33
21 Oct 64	07 38 31.0	Hebgen Lake	44.8N	111.6W	5.8	33
22 Oct 64	16 00 00.0	SALMON	33.4N	89.6W	4.6	
25 Nov 64	02 50 05.0	W. Virginia	37.4N	81.5W	4.5	
06 Mar 65	21 08 49.9	Missouri	37.4N	91.1W	5.3	33
03 Jun 65	19 30 25.7	Wyoming	43.6N	106.5W	4.7	33
15 Jul 65	14 16 07.0	Off E. coast	37.3N	74.4W	5.1	

were similarly reduced by the regional fall-off rate of the phase that can be written as (Alsup, 1970) $\Delta^{-2} \exp(-\pi f \frac{\Delta}{8.1} \cdot \frac{1}{Q})$ where the values f = 3Hz and Q = 1000 were used. The effect on P_g is .26 amplitude units. For P_g, f = 2.5 was used in the same formula; the frequencies used were determined by measuring the records. After correcting for event magnitudes we obtained histograms for the two types of sites; these are shown in Figures 6 and 7 , respectively. The site effect due to sediments appears to be quite large, .33 magnitude units.

In addition to effects on amplitudes, the envelope shapes of L_g are also changed by sediments. The observed effect is similar to that observed at Yucca Flats, that is, the coda length of L_g increases on sediments and the maximum amplitude is also reached at a later time. This is illustrated by Figure 8. This figure shows plots of the arrival times of the envelope maximum and the 1/2 max point, connected by lines, as functions of epicentral distance. The two kinds of symbols denote the two types of sites. The tendency is evident for the sedimentary sites to have longer L_g codas as well as delayed arrivals of the maximum of the envelope.

The effect on envelope shapes cannot, at present, be explained by resonances in small local structures as at NTS since most of our sedimentary sites are located in broad sedimentary basins.

Z. A. Der
A. O'Donnell
M. Marshall

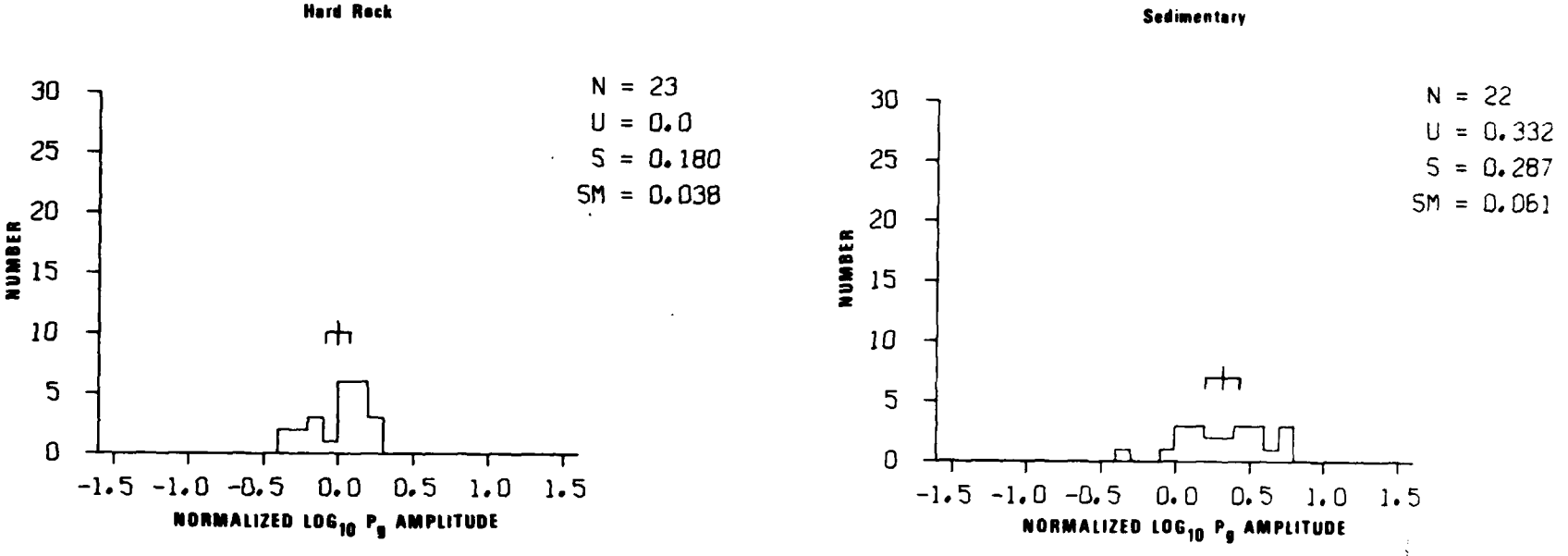

Figure 6. Histogram of the distance and magnitude corrected P_g amplitudes at hard rock (left) and sedimentary sites. Explanation of symbols U - mean, S - standard deviation, SM - standard deviation of the mean.

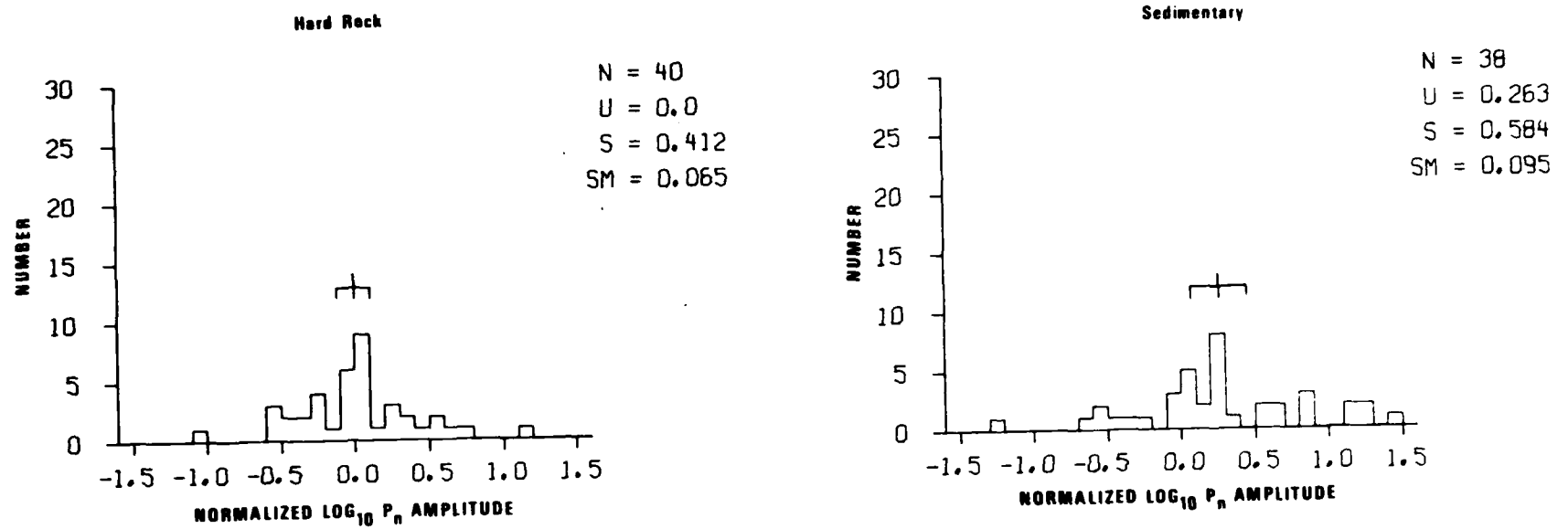

Figure 7. Histogram of the distance and magnitude corrected P_n amplitudes at hard rock (left) and sedimentary sites. Explanation of symbols U - mean, S - standard deviation, SM - standard deviation of the mean.

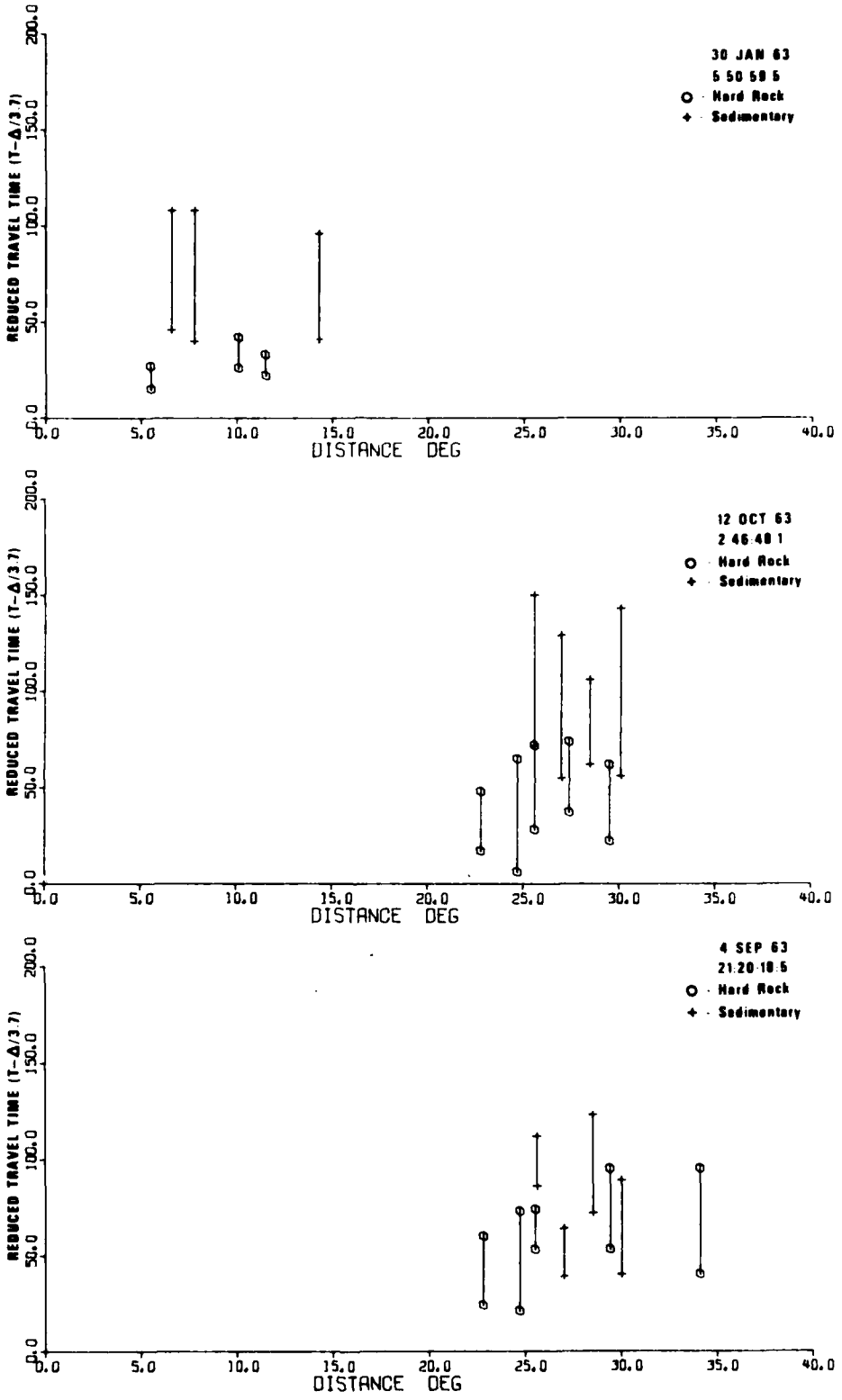

Figure 8. Arrival times of the L_g maxima, the 1/2 max point (connected by bars) at hard rock (circle) and sedimentary (+ sign) sites plotted against distance. The L_g maxima arrive later and the coda is longer at sedimentary sites.

C. Phase Velocity Versus Depth Studies

Apparent phase velocities at the maximum of L_g appear to be diagnostic of the source depth, and thus have a discrimination potential.

In an early study, Barley (1978) showed that apparent phase velocities measured across the Yellowknife array tended to increase with increasing source depth. A ray theory explanation of this phenomenon is that deep sources are associated with rays of deeper penetration in the earth, with correspondingly higher apparent velocities along the surface. Another manifestation of this idea, the change of L_g envelope shapes with depth, deeper rays being associated with faster group velocities was demonstrated by Noponen and Burnetti (1980). To test this idea, we have measured apparent phase velocities of L_g across the Alaskan array BFAK. Although the amount of data processed is small, it tends to confirm Barley's findings. In Figure 9 we show some phase velocity measurements versus source depth at the Alaskan array BFAK. The phase velocities were taken from F-K spectra, with fairly high F values indicating good coherence across the array. Figure 10 shows some phase velocities computed from synthetic seismograms computed from various source depths, also showing the same tendency. We are in the process of collecting a much larger data set to investigate the stability of the method observationally as well as theoretically. Clearly, in order to be usable, the sensitivity of the method to various crustal structures and source mechanisms must be known.

Z. A. Der
P. Klouda

D. Scattering and Q Effects

Envelope shapes of L_g are likely depth discriminants. Site effects or the time domain shapes of L_g are caused by resonances in local, two and three dimensional geological structures and by scattering at near surface inhomogeneities. The relative importance of these effects must be understood.

Codas of near earthquakes have been described in terms of backscattering from random inhomogeneities, Aki (1969) and Aki and Chouet (1975). In our previous work, we described the site amplification and coda lengthening in terms of resonance in a basin filled with low-velocity sediments. Band-pass filtering of L_g waves showed that the coda length depends on frequency. Figure 11 shows an example of this at Yucca Flats. Since all sites show this phenomenon, it appears that there is a contribution to the energy in the L_g

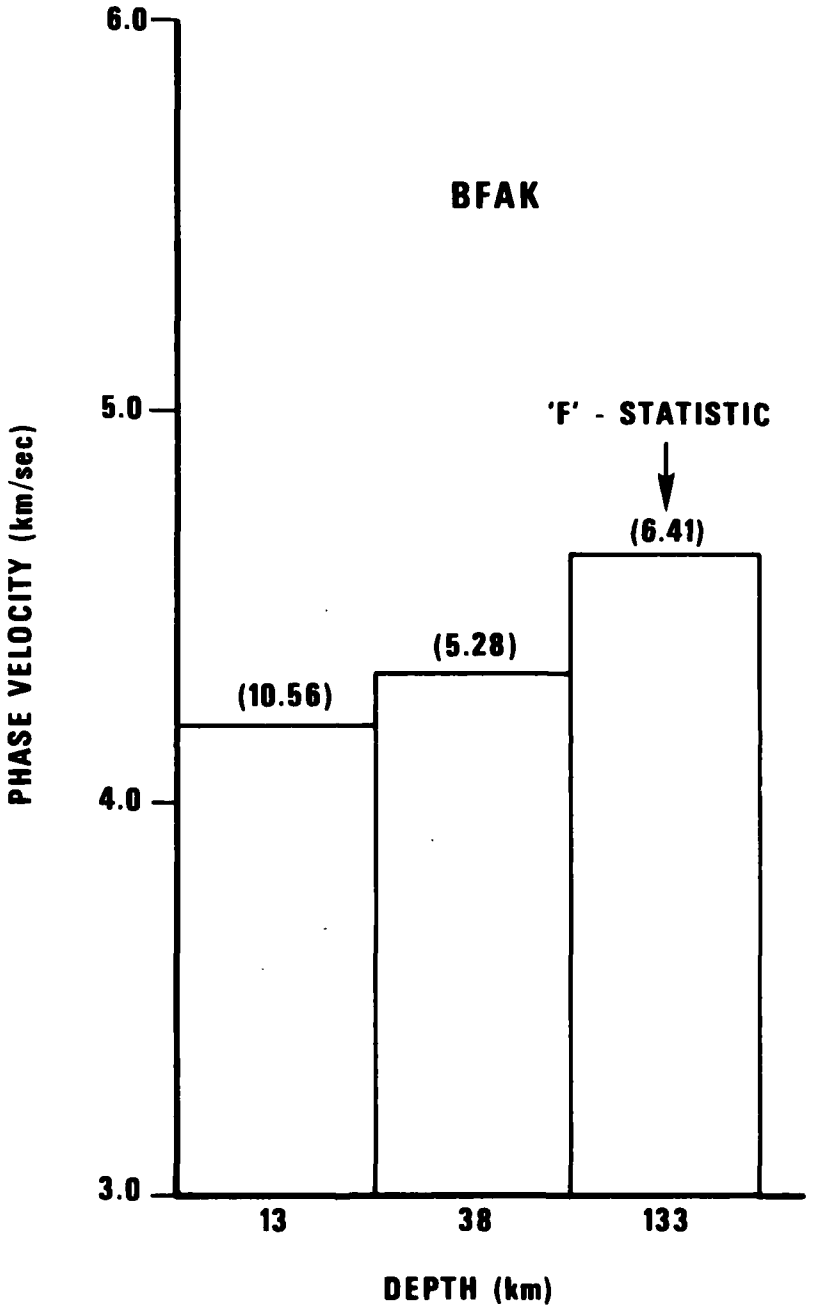

Figure 9. Apparent phase velocities in vertical component L_g at the Alaskan array BFAK as a function of source depth.

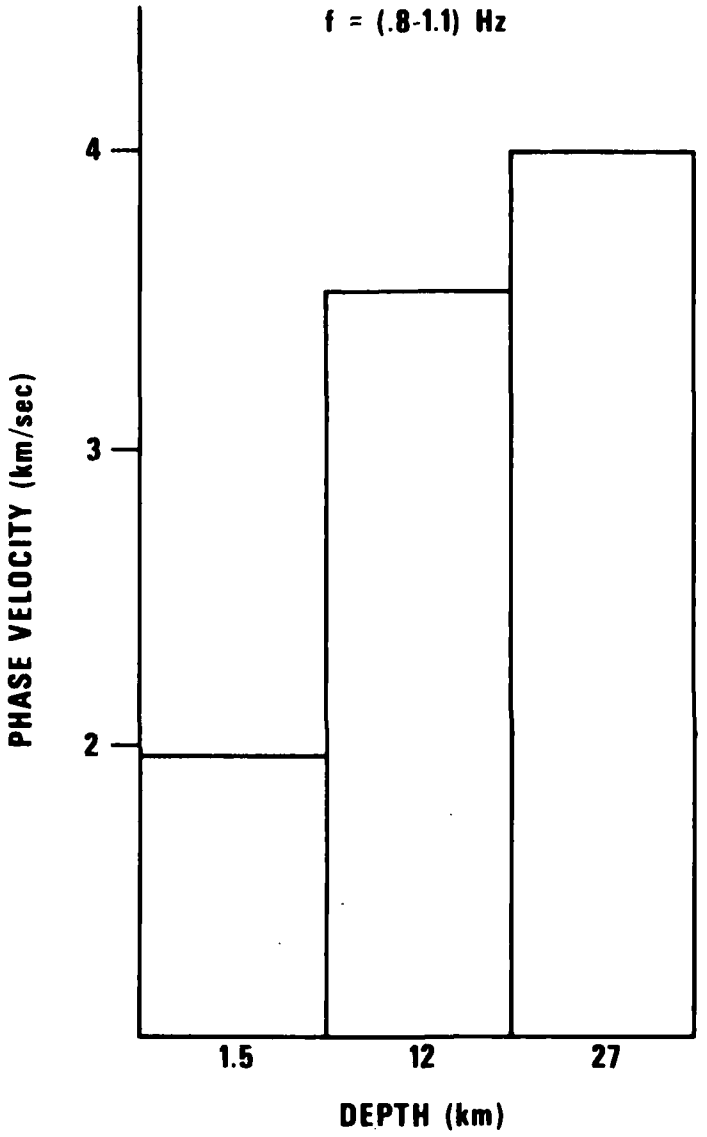

Figure 10. Apparent phase velocities (c) of synthetic L_g (transverse) seismograms versus source depth illustrating the principle of dependence of c on source depth. This figure is not directly comparable to Figure 9 since the component of motion as well as the applicable crustal structure is different.

wavetrains from scattered waves that should be better understood if L_g is used for yield estimation. To evaluate this effect, we have developed computer programs that:

- Simulate the resonances in a 2D basin structure with variable velocity and Q structure using finite difference methods.
- Predict envelopes in scattered wavetrains with various assumptions about Q structure, scattered and primary wave velocities. The approach is similar to that applied by Aki (1969).
- Compute synthetic seismograms using mode theory. The SH (Love) case is currently operational. Programs to compute Rayleigh mode synthetics are being developed currently. Details of this development effort are given in a separate section of this report.

Observations of L_g, P_g and P_n amplitude anomalies and changes in wave envelopes will be modeled at the shield sites being studied, and compared to synthetic, finite difference and scattering models.

Z. A. Der
A. O'Donnell
T. W. McElfresh

E. Amplitude-Distance Relationships for Regional Phases Based on Analysis of Soviet Data

Amplitude distance relationships of the various regional phases must be known for yield estimation and discrimination using amplitude ratios of such phases.

Perhaps the most useful single source of Russian data on regional phases is the monograph by Antonova et al (1978). Other sources used in this study are Nersesov and Rautian (1964), Ruzaikin et al (1977), and Shishkevish (1979). Most of the data in these studies comes from seismographic stations in and near the Tien Shan region and in the region east of 70°E, bordering China and Mongolia. Most of this area has generally been recognized as one of efficient propagation of Lg (Gupta et al, 1980; Ruzaikin et al, 1977).

The amplitude-distance curves of all regional phases (Pn, Pg, Sn and Lg) are highly variable from one region to another and even from one direction to another. Nersesov and Rautian used data from a number of stations in the region between the Pamirs and the Lena River and found the spatial attenuation of all regional phases to vary significantly both as a function of location and direction (see Figures 11 through 14, Nersesov and Rautian, 1964). Amplitude-distance relationships for different frequency bands at a station in southeastern Kazakh, central Asia again showed significant variations with both azimuthal direction and average passband frequency (Antonova et al, 1978). The amplitude variations in all these studies are relatively the least for the phases Lg and Pg although scatter by a factor of about 2 is rather common even for these two phases. The most stable and the largest amplitude phase is generally Lg, observed to distances of 3000 km or greater. The next most stable and large amplitude arrival is Pg recorded to a distance of only about 1000 km.

Figure 12 shows composite or average amplitude curves of Lg, Pg, Sn and Pn from 40 crustal earthquakes originating in North Tien Shan and recorded by seismographic stations equipped with SKM-3 instruments in the same region (Shishkevish, 1979). The SKM-3 seismograph is a short-period system with flat response in the period range 0.1 sec to about 1.2 sec and peak response at about 1.4 sec. The peak amplitudes have been normalized to a standard magnitude and distance. The two largest-amplitude phases are Lg and Pg and, on the average, Lg is about three times as big as Pg.

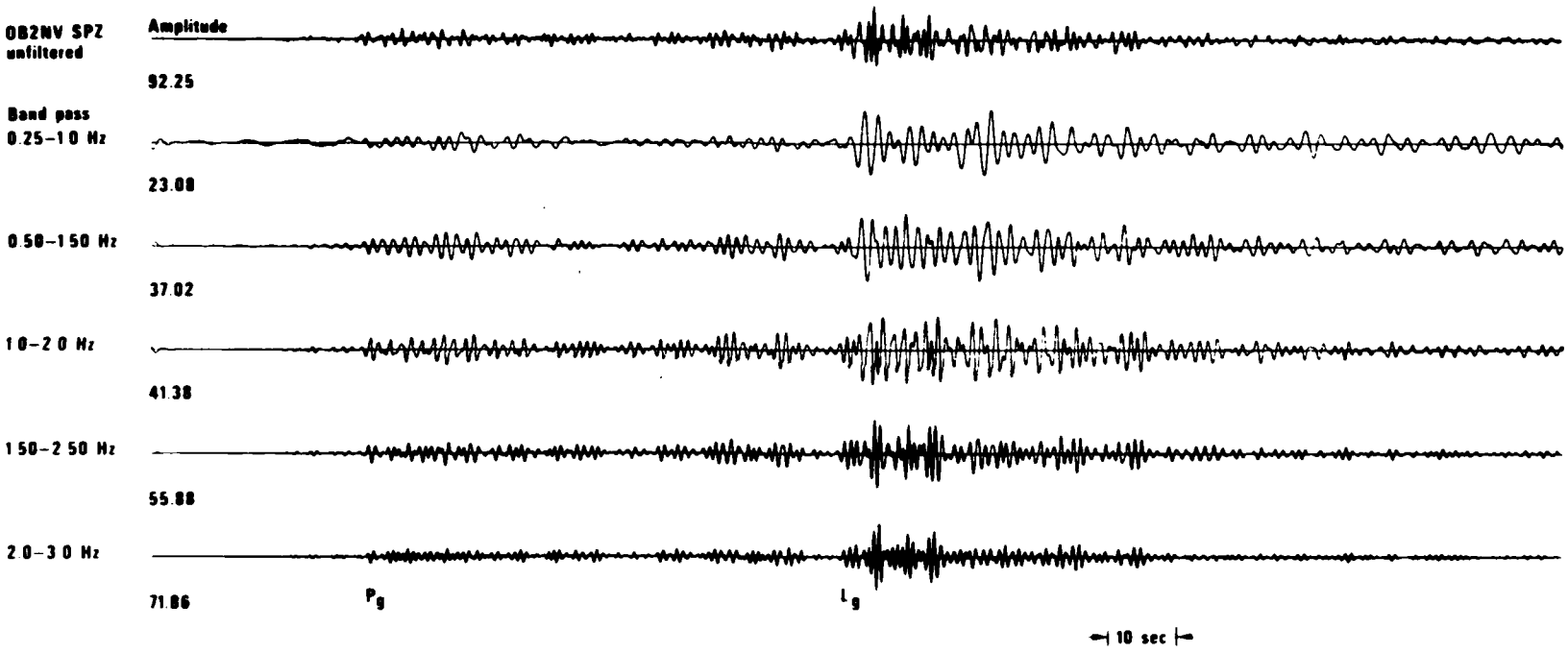

Figure 11. Band pass filtered seismograms containing P_g and L_g phases at the SDCS station OB2NV at NTS. The falloff rate of the P_g and L_g codas is the greatest at high frequencies, an apparent Q effect.

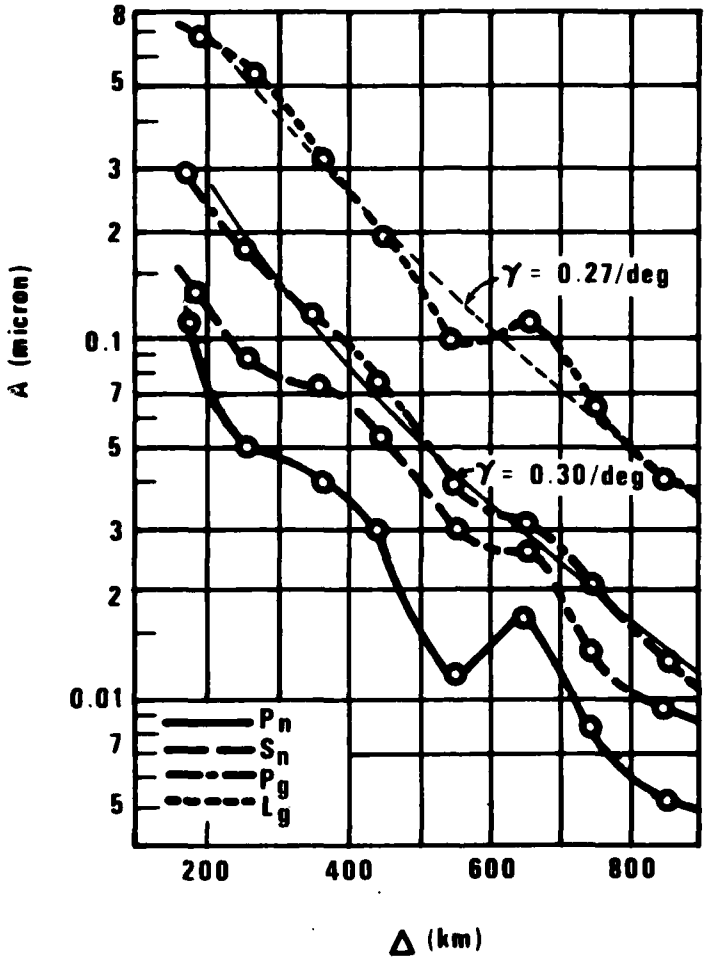

Figure 12. Average amplitude curves of regional phases L_g, P_g, S_n, and P_n for the North Tien Shan region (after Figure 9, Shishkevish, 1979). The two thin curves represent theoretical least-squares fit to the observed data.

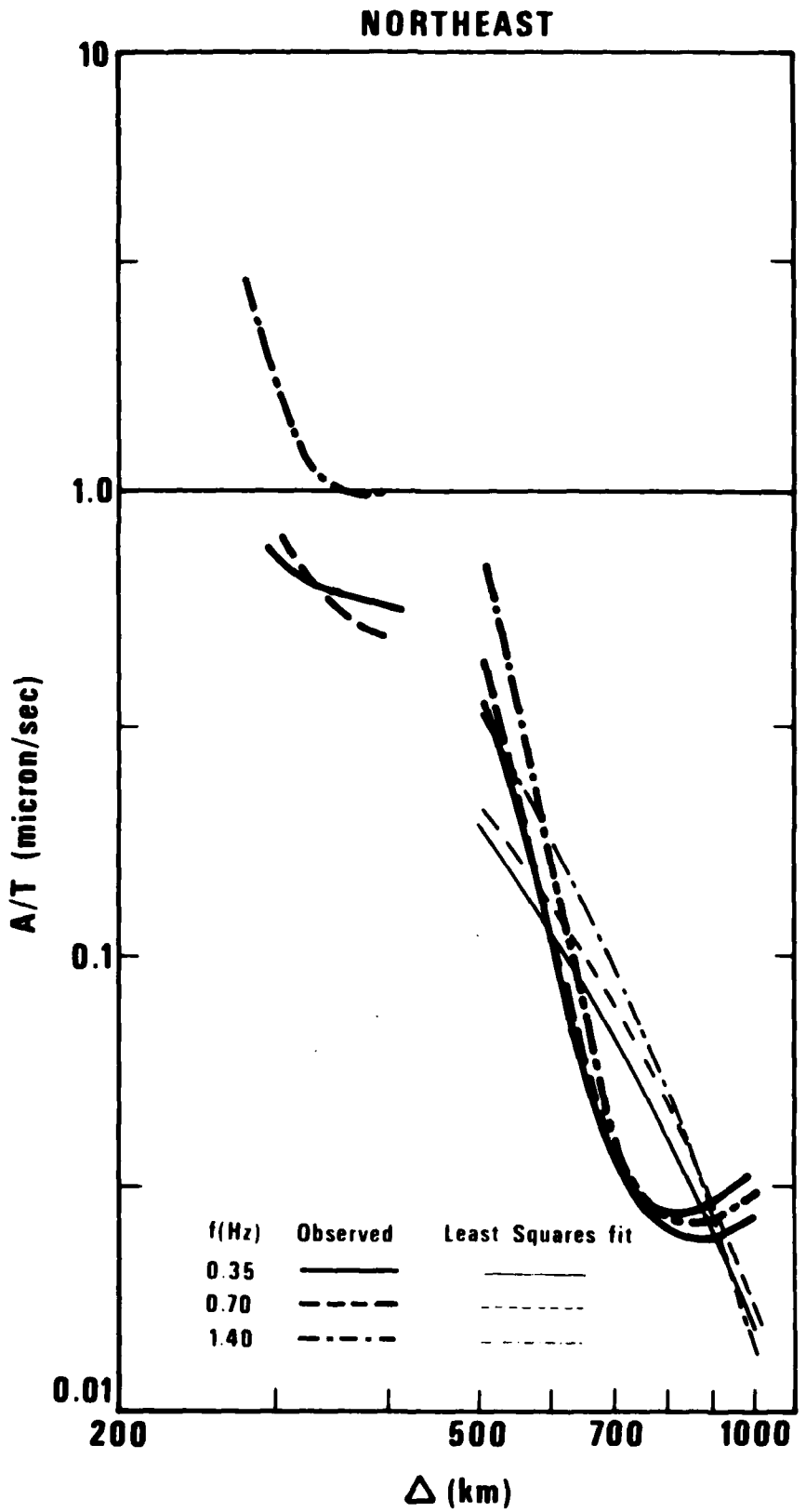

Figure 13. Spectral amplitude-distance curves of P_g along the Northeast direction (after Figure 20, Antonova et al, 1978). The thin lines represent theoretical least-squares fit to the observed data.

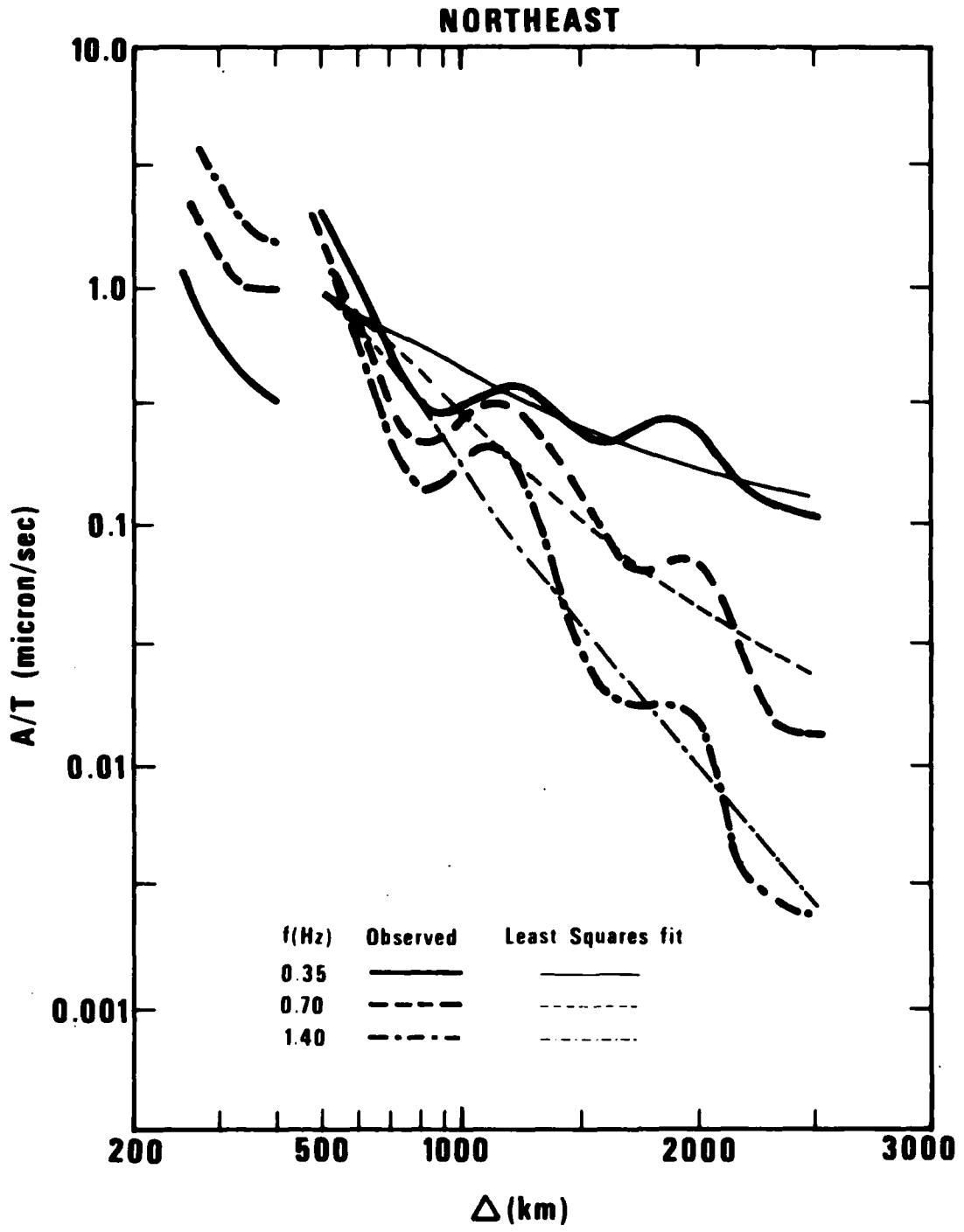

Figure 14. Spectral amplitude-distance curves of L_g along the Northeast direction (after Figure 23, Antonova et al, 1978). The thin lines represent theoretical least-squares fit to the observed data.

Lg may be regarded as a higher-mode surface wave traveling with minimum group velocity (Nuttli, 1973) so that the time-domain amplitude, A varies with distance, Δ as

$$A = K\Delta^{-\frac{1}{3}} (\sin \Delta)^{-\frac{1}{2}} e^{-\gamma\Delta} \qquad (1)$$

where Δ is in degrees, γ is the coefficient of anelastic attenuation and K is a constant. Taking logarithms to base 10, equation (1) gives

$$\log A + f(\Delta) = \log K - \gamma\Delta \log e \qquad (2)$$

where $f(\Delta)$ is a known function of Δ. Equation (2), a linear equation suitable for least-squares curve fitting, yielded a γ value of about 0.27 per degree for the Lg amplitudes in Figure 12. Recent data suggest that Pg may also be regarded as a dispersed surface wavetrain so that equation (1) may be applicable (e.g. Nuttli, 1980). Using data on Pg amplitudes in Figure 12, a mean value of $\gamma = 0.30$ per degree was obtained. Therefore the attenuation coefficients for Lg and Pg, based on data in Figure 1, are nearly equal. These values of γ for Lg lie somewhere between $\gamma = 0.07$/deg for 1-sec-period Lg in the eastern United States (EUS) and $\gamma = 0.6$/deg for southern California (Nuttli, 1973).

Data on amplitude-distance curves of Lg and Pg for different frequency bands (Antonova et al, 1978) provide valuable insight into the generation, propagation and spectral characteristics of the two important regional phases. Recordings of earthquakes by a seven-channel ChISS station located at Talgar (approximately 43°N and 77°E) in Tien Shan were used in these studies. The ChISS station is a frequency-selection seismograph station in which the vertical component of ground velocity is passed through a system of band-pass filters so that the amplitude of each recording is proportional to the vertical component of ground velocity in a particular frequency band (Rautian et al, 1978). The epicentral locations of earthquakes were divided amongst four azimuthal directions relative to the Talgar station: Northeast (Zaysan, Altay, Sayan, Pribaykal and Transbaykal), East (Dzungaria, northwest China and Mongolia), South (Pakistan, Nepal and India) and West (South Tien Shan, Pamirs, Tadzhik, Iran, and the Caucasus).

A comparison of amplitude-distance curves of L_g and P_g, (Figures 13 and 16 after Antonova et al, 1978) shows several interesting features. For propagation along the same direction, the amplitude-distance curves of Pg and Lg have

similar trends. Figures 13 and 14 show the amplitude-distance curves, normalized to magnitude 5 earthquakes, along the Northeast direction for three frequency bands for Pg and Lg, respectively. Amplitudes of both phases attenuate slowly for epicentral distance, Δ less than 400 km and much more rapidly for Δ greater than 500 km. Both sets of curves show a minimum at Δ about 800 to 900 km. Figure 15 and 16 show results for Pg and Lg, respectively for earthquakes along the West direction. An examination of Figures 13 to 16 suggests that the attenuation of both Pg and Lg varies greatly with direction.

Assuming the validity of equation (1), the absorption coefficient, γ and corresponding values of the quality factor, Q given by

$$Q = \frac{\pi f}{\gamma u} \tag{3}$$

where u is the group velocity, have been obtained for the amplitude-distance curves in Figures 13 to 16. The values of u for Lg and Pg are taken to be 3.5 km/sec and 5.7 km/sec, respectively (see Table III, Gupta et al, 1980). The results obtained by the least-squares linear regression of observed data are given in Table II, in which the standard deviation error in γ is also indicated. In Figures 13 and 14, data for $\Delta < 500$ km is rather erratic and therefore not used in the analysis. Based on the somewhat limited data in Table II, the following inferences may be drawn: (1) Q increases substantially with frequency for both Pg and Lg, for $\Delta \leq$ 1000 km, (2) Q(Pg) is less than Q(Lg) by a factor of 2 to 3 for a given frequency and direction of propagation, (3)Q (Lg) increases substantially for $\Delta >$ 1000 km, and (4) Lg travels more efficiently (higher Q) along the Northeast direction than along the West direction whereas Pg is less efficient for propagation along the Northeast direction than along the West direction; this effect is more pronounced for higher frequencies.

A strong increase in Q with frequency has previously been noted for Lg by Molnar et al (1976) for the region between Talgar and Lake Baykal (Shishkevish, 1979). Using data from underground nuclear explosions at Nevada Testing Site, Press (1964) reported Q values for Lg greater than for Pg by a factor of 2 to 3. Rautian et al (1978) pointed out that Soviet scientists have often observed Q for S waves to be greater than Q for P

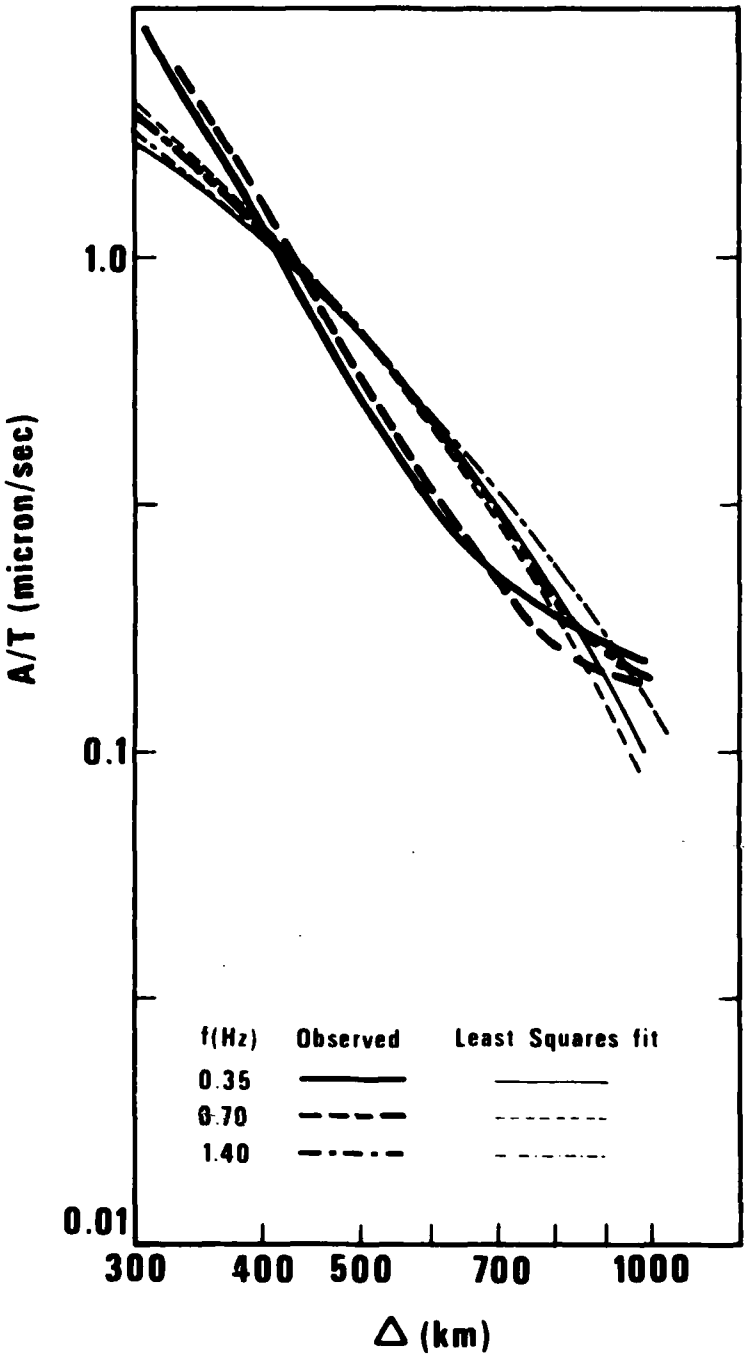

Figure 15. Spectral amplitude-distance curves of P_g along the west direction (after Figure 20, Antonova et al, 1978). The thin lines represent theoretical least-squares fit to the observed data.

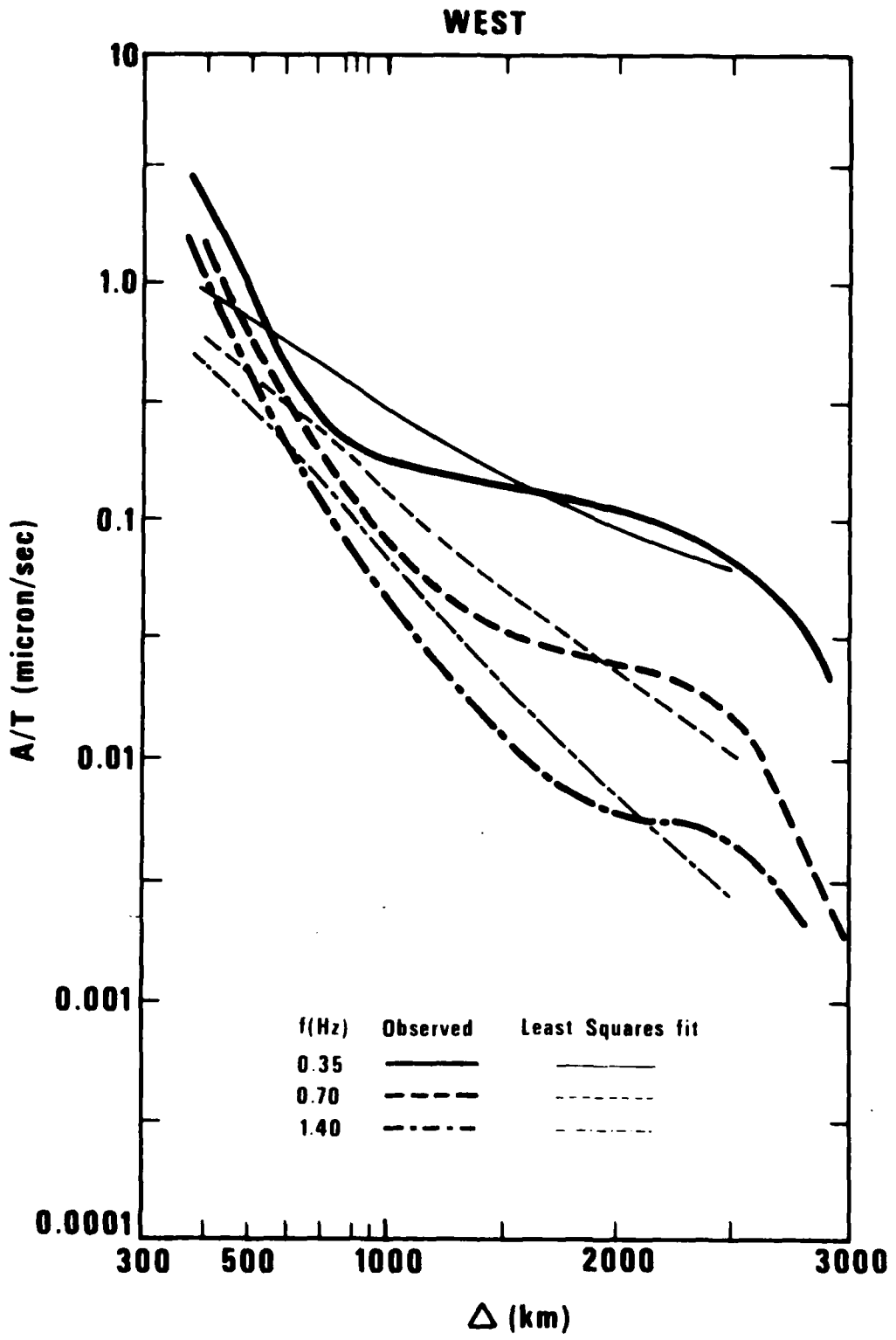

Figure 16. Spectral amplitude-distance curves of L_g along the west direction (after Figure 23, Antonova et al, 1978). The thin lines represent theoretical least-squares fit to the observed data.

TABLE II

SPATIAL ATTENUATION AND CORRESPONDING Q VALUES

Direction	Phase	Range of epicentral distance (km)	Mean frequency (Hz)	γ (per degree)	Q
NE	P_g	500 to 1000	0.35	0.43 ± 0.15	50
			0.70	0.42 ± 0.18	100
			1.4	0.57 ± 0.20	150
	L_g	500 to 1000	0.35	0.29 ± 0.09	120
			0.70	0.25 ± 0.12	280
			1.4	0.36 ± 0.13	390
	L_g	500 to 1000	0.35	0.04 ± 0.02	925
			0.70	0.14 ± 0.02	495
			1.4	0.26 ± 0.02	540
W	P_g	300 to 1000	0.35	0.31 ± 0.06	70
			0.70	0.35 ± 0.06	125
			1.4	0.27 ± 0.01	325
	L_g	350 to 1000	0.35	0.29 ± 0.07	120
			0.70	0.35 ± 0.04	200
			1.4	0.44 ± 0.06	320
	L_g	350 to 2500	0.35	0.06 ± 0.02	580
			0.70	0.13 ± 0.02	550
			1.4	0.19 ± 0.02	725

TABLE III

REGIONAL EVENTS AT RKON

#	Date	Origin Time	Coordinates		Geographic Region	Mb	Δ°	φ°
1	11 Mar 78	23:57:45.3	31.9N	114.7W	Gulf of California	4.7	24.5	227
2	12 Mar 78	00:30:17.4	32.0N	115.0W	Southern California	4.1	24.5	227
3	12 Mar 78	18:42:24.1	32.0N	114.9W	W. Arizona-Mexico border	4.7	24.5	227
4	09 Mar 76	14:00:00.1	37.310N	116.364W	S. Nevada*	6.0	21.0	238
5	20 Mar 76	00:47:27.3	73.194N	68.899W	Baffin Bay	4.5	24.6	16
6	25 Mar 76	00:41:20.5	35.59N	90.48W	Arkansas	4.9	15.4	170
7	22 Apr 76	04:21:39.1	43.636N	127.005W	Off Coast of Oregon	4.2	23.5	265
8	26 Jul 76	10:45:28.2	49.022N	114.179W	Western Idaho	4.3	14.9	254
9	31 Jul 76	22:32:10.5	26.242N	110.338W	Gulf of California	4.8	27.7	213
10	10 Aug 76	13:54:57.2	45.029N	106.569W	Montana	3.4	10.4	241
11	12 Aug 76	06:28:59.	50.62N	123.01W	British Columbia	3.8	18.4	280
12	02 Sep 76	13:16:11.0	48.205N	122.761W	Washington	4.3	18.9	273
13	03 Sep 76	04:18:16.2	44.041N	106.154W	Wyoming	4.8	10.8	235
14	13 Sep 76	18:54:37.1	36.604N	80.810W	North Carolina	3.3	16.9	142
15	16 Sep 76	10:14:39.0	76.136N	108.384W	Qu. Elizabeth Isls	4.6	25.9	352
16	25 Sep 76	14:06:56.6	35.61N	90.45W	Arkansas	3.6	15.4	170
17	19 Oct 76	07:24:34.0	44.795N	110.697W	Yellowstone Park, Wyo.	5.3	12.9	248
18	23 Oct 76	20:58:18.1	47.82N	69.79W	Gaspe Peninsula	3.8	15.8	91
19	27 Nov 76	00:24:46.1	44.639N	111.142W	Hebgen Lake	3.3	13.2	248
20	08 Dec 76	14:40:59.4	44.760N	110.793W	Yellowstone Park, Wyo.	5.5	13.0	248
21	11 Dec 76	07:05:00.9	38.12N	91.07W	Missouri	4.2	12.8	170
22	13 Dec 76	08:35:54.6	37.798N	90.236W	Eastern Missouri	3.5	13.3	168
23	19 Dec 76	17:10:15.7	44.772N	110.800W	Yellowstone Park, Wyo.	4.9	13.0	248
24	20 Dec 78	01:34:16.0	44.842N	110.827W	Yellowstone Park, Wyo.	4.4	12.9	249
25	13 Jan 78	08:25:34.5	52.8N	132.0W	Queen Charlotte Isl.	4.4	23.5	289
26	05 Feb 78	16:07:09.9	78.4N	107.8W	Queen Elizabeth Isls.	4.9	28.0	354
27	23 Feb 78	16:59:59.3	36.9N	45.9W	California-Nevada border	5.6	21.1	237
28	04 Mar 78	19:13:33.5	50.3N	114.4W	Alberta Province, Canada	3.5	13.1	275
29	03 Jan 77	22:56:48.6	37.55N	89.79W	Cape Girardeau, Mo., region	5.0	13.6	166
30	27 Jan 77	00:51:05.0	66.790N	135.433W	N. Yukon Territ., Canada	4.7	26.1	323
31	30 Sep 77	10:19:21.	40.518N	110.436W	Utah	5.0	15.5	234

* explosion

waves; as this is opposite to observations of attenuation in the upper mantle, it is a puzzling result. Q(Lg) increasing with epicentral distance is, as mentioned earlier, probably due to deeper penetration of the crust. The opposite directional effects suggesting that an increased efficiency of Lg may be accompanied by a decreased efficiency of Pg and vice versa is very hard to explain. However, the presence of strong Lg and weak Pg in EUS and weak Lg and strong Pg in WUS are perhaps manifestations of the same puzzling feature of Pg and Lg phases. Most of the observed data came from a single station so that the results should be considered preliminary.

I. N. Gupta

J. A. Burnetti

DETECTION OF REGIONAL PHASES

The purpose of this study was to devise a regional event detector making use of the fundamental-mode surface-wave processor developed by Smart (1977). The study has enabled us to explain the past success of the processor as an azimuth estimator, when applied to L_g phases.

A test data set of 32 events was collected at RKON, well distributed azimuthally about that station (Table III), Figure 17. Signal and noise spectra were computed for all the L_g phases. The noise spectra were found not to vary significantly over the seasons. Figure 18 shows the spectra of four events, the two highest and the two lowest peak frequencies in the data set. It also shows composite noise spectra by seasons. It can be seen that the noise spectra peak below 0.4 Hz, whereas all signal spectra peak above that frequency. (The instrument response has not been removed for these spectra. Also, below 0.2 Hz the spectra are probably system noise.) In general, the low-frequency signals were those which transversed complex mountainous regions on their way to RKON, e.g., events from California, Oregon, Washington, and British Columbia.

A modified version of the Smart processor was used which estimates particle motion ellipticity. Previously ellipticity was an input parameter. The frequency band examined was 0.5 and 3.0 Hz. The L_g window for each case was hand picked by an analyst. Good back azimuths were obtained in general: the rms error was 6.7°. Some of the low-frequency events yielded the least accurate estimates.

We attempted to find a parameter for detection, i.e., one which separated signals from the noise. The parameters investigated were: the F-statistic, the mean recurrence period, and the derivative $\frac{\partial^2 E}{\partial \phi^2}$, where E = error and ϕ = back azimuth (see Smart, 1977). The rms excursions for the model in the vertical, radial, and transverse directions, denoted by Z, R, and T, were also examined.

The derivative did not follow a discernible pattern. The F-statistic and mean recurrence period were consistently low for both noise and signal and did not separate them (see Figure 19 for F-statistic histogram). The best discriminator was the quantity T/R, but the separation of the populations was not clear enough to provide a reliable detection parameter (Figure 20). It was observed that $T/R < 2.0$, when it occurred, accompanied poor azimuthal

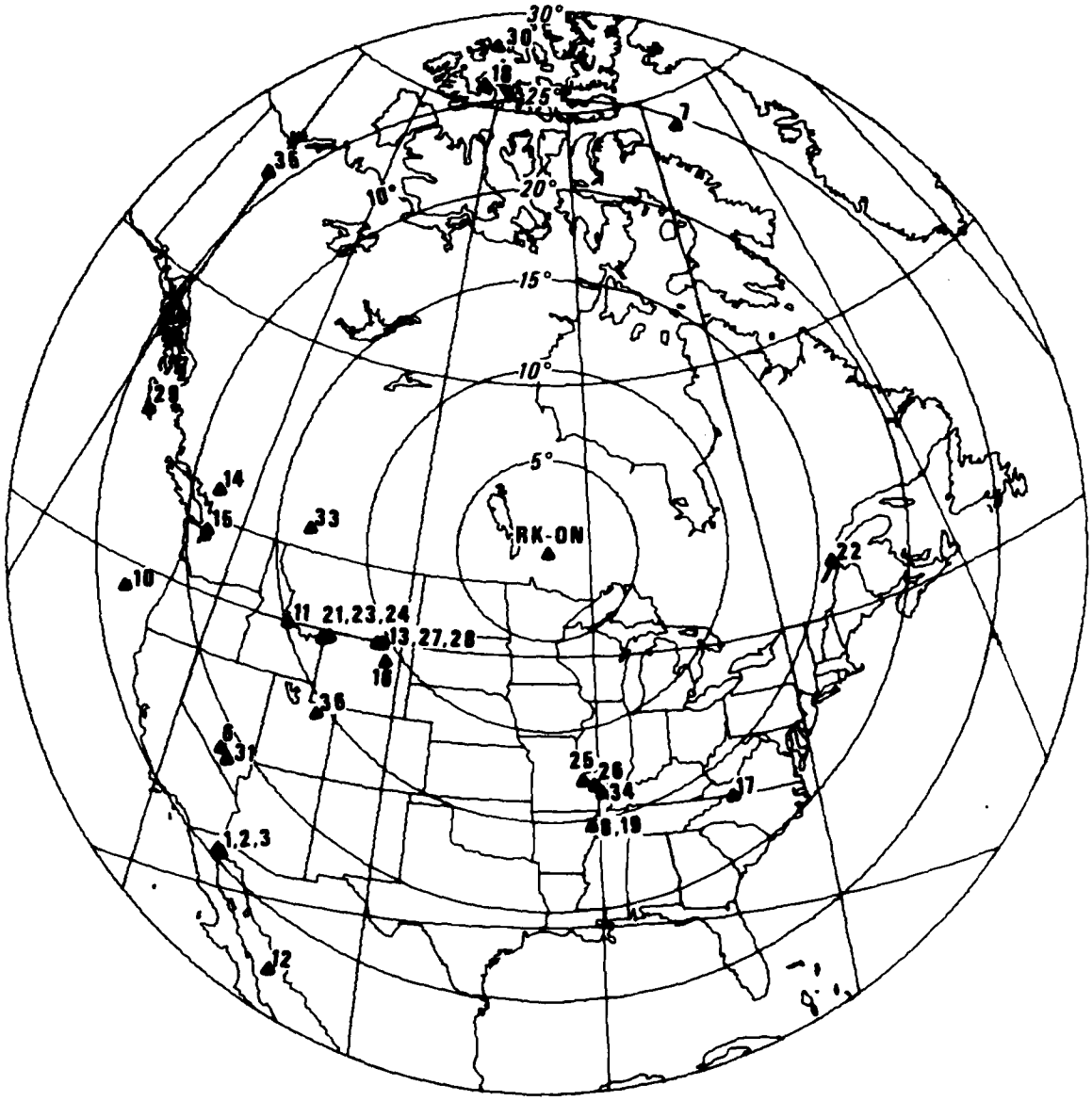

Figure 17. Map showing the location of RKON and of the events used in this study.

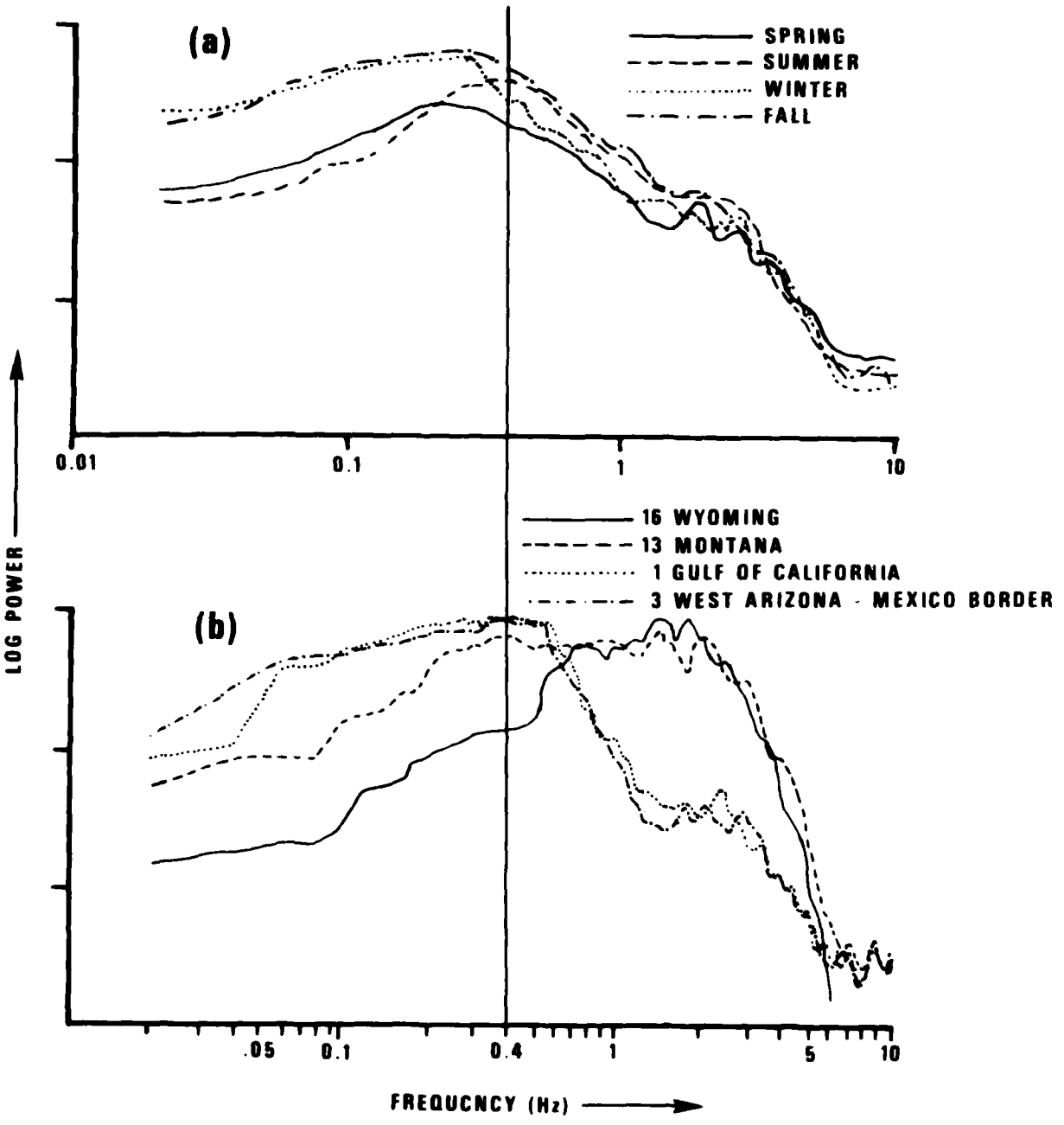

Figure 18. (a) Composite noise spectra for RKON, for four seasons.
(b) Peak-normalized spectra of the lowest- and highest-frequency event nos. 1, 3, 13 and 16.

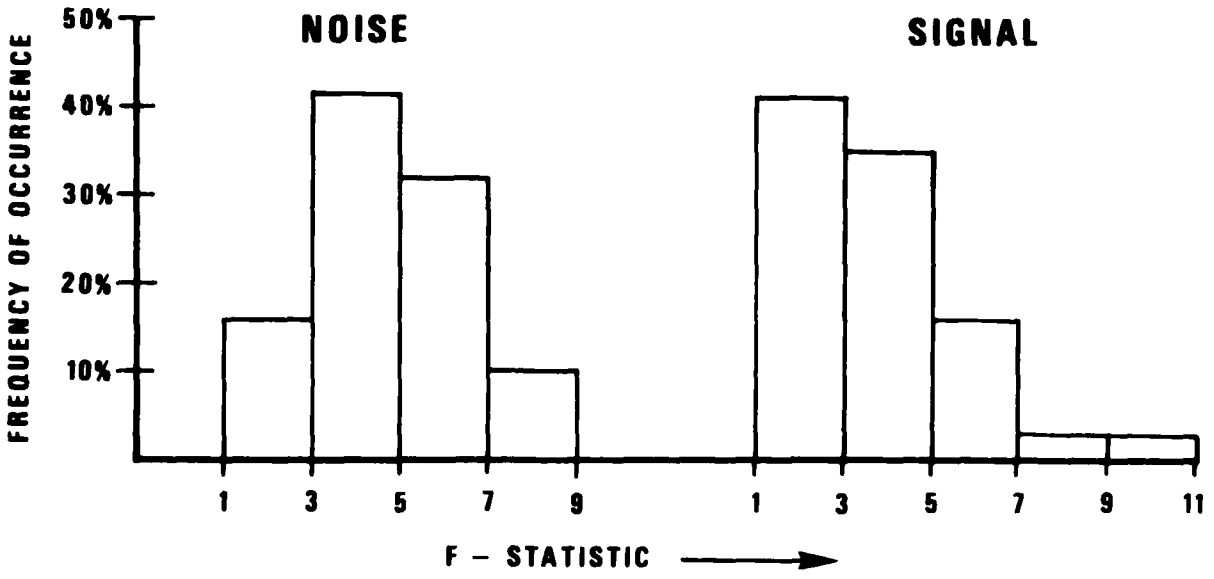

Figure 19. F-statistic for noise and L_g phases for the frequency band 0.1 to 6.0 Hz show negligible separation of populations.

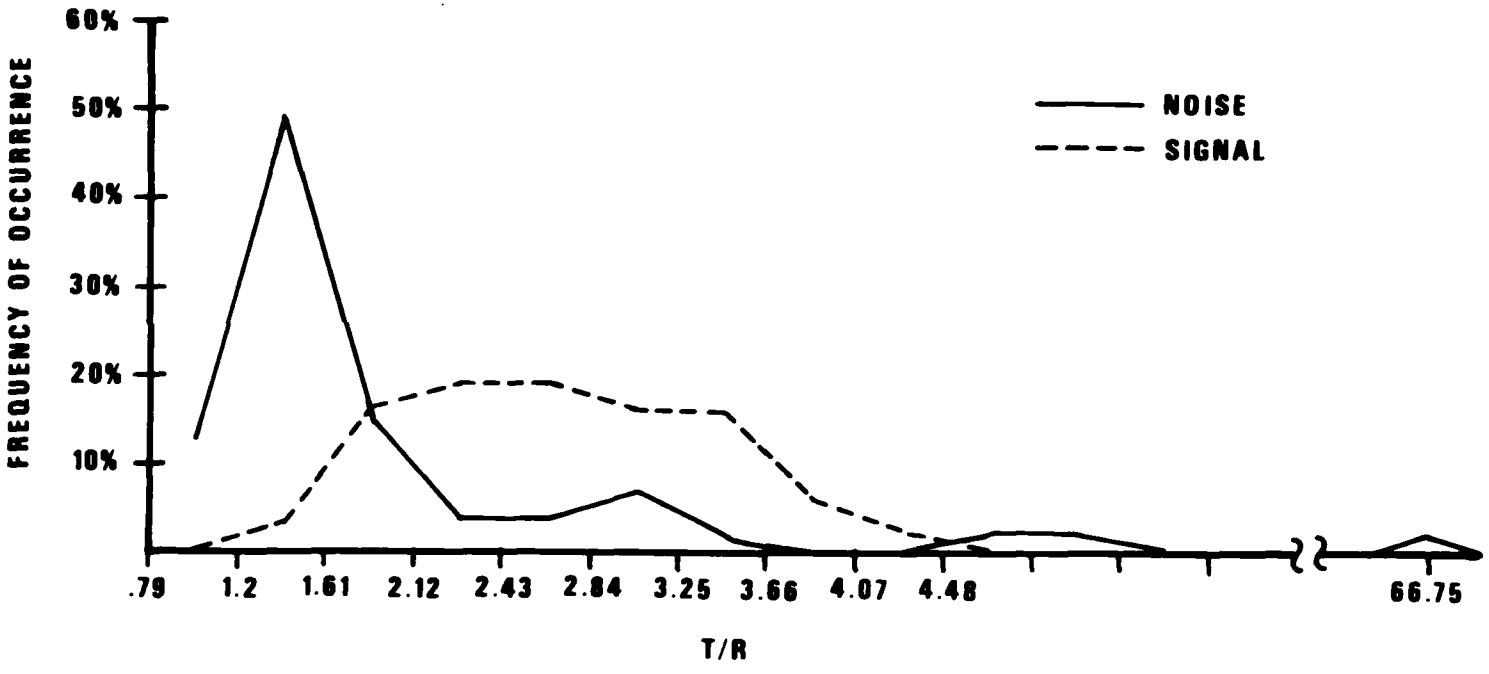

Figure 20. Separation of noise and signal by T/R.

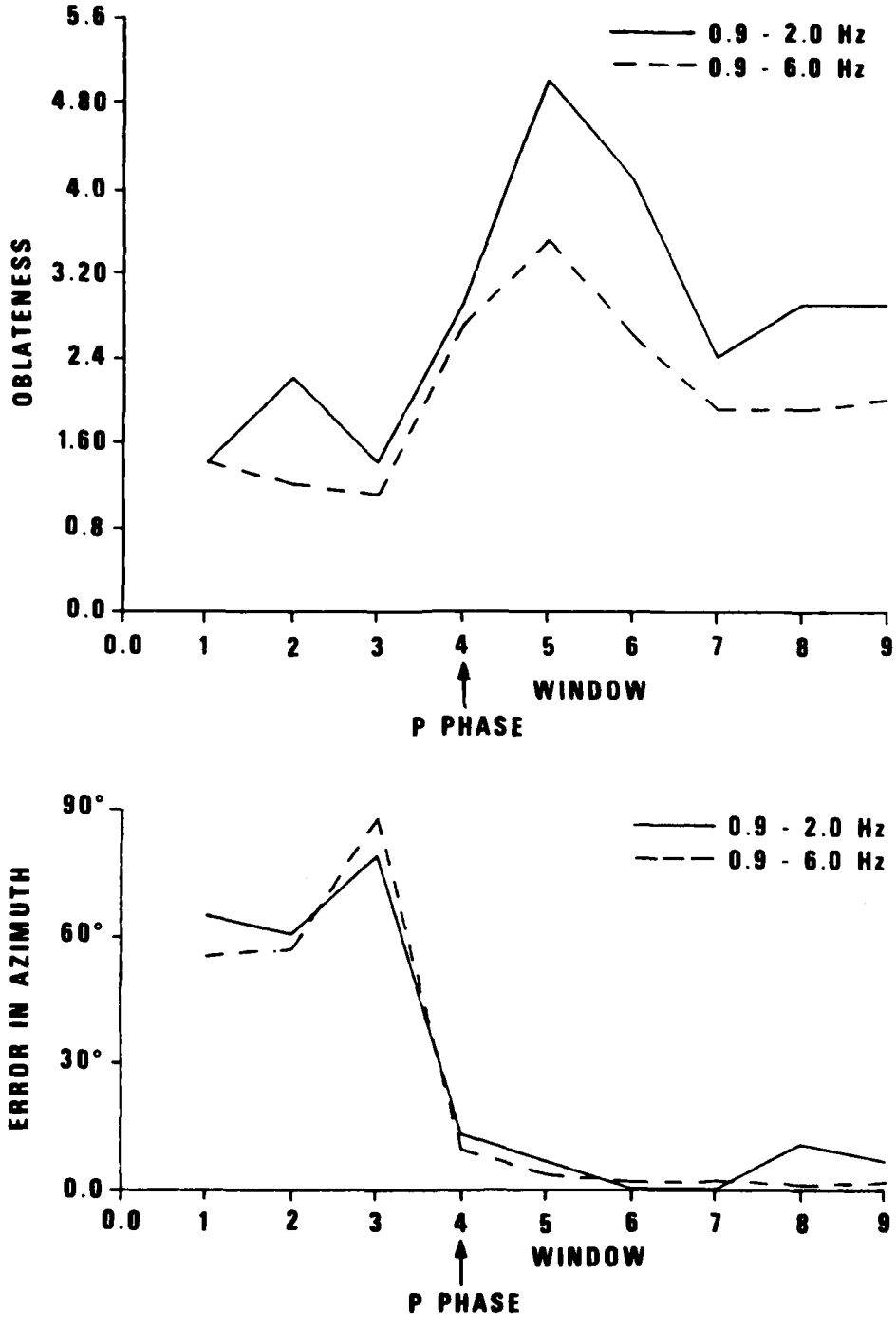

Figure 21. Oblateness values and error from true azimuth as the processor moves through successive 128-point windows, for event 13 (Montana). Two bands are displayed here.

estimates, i.e., > 10.0° error, and that the smaller T/R, the larger the azimuthal error.

These observations suggested that the figure traced by the particle motion in the horizontal plane might serve to indicate signal azimuth. An algorithm was coded to find in each time window the orientation in the horizontal plane in which the rms excursion, in the frequency band of interest, was the least. The azimuth of that orientation was, on the average, as good an estimate of surface wave origin as the back azimuth from the original coherent processor. Moreover, it was more stable. In low signal-to-noise records, where T/R fell below 2.0, the estimated azimuth was more accurate than that of the coherent processor. All this appears to explain why the Smart processor has been successful in estimating L_g azimuths, but unsuccessful in <u>detecting</u> L_g phases. The azimuth estimations have been controlled by the dominant transverse Love component, but the F-statistics have been kept low by the incoherence between the vertical and radial components, incoherence resulting from the mixing of Rayleigh modes, the fundamental and higher modes. Thus, the Smart processor operating on L_g waves functions as an incoherent processor.

The results suggested another use of the elongation figure described by the particle motion, that is, to flag the arrival of P-waves and indicate their azimuths. Time windows of 6.4 seconds--an order of magnitude smaller than those for the L_g waves--were used to search in the vicinity of the expected P arrivals. The axis of elongation was taken to indicate back azimuth, and the amount of elongation, that is, the ratio of the long axis to the short axis, was taken as the index of signal presence. Taking that ratio at 2.4 as the detection threshold, in the band 0.9 to 6.0 Hz, 80% of the signals were detected with a false alarm rate of 28 per hour. The average azimuthal error was 6.0 degrees, and in the case of the low-frequency, low signal-to-noise events these P azimuthal estimates were markedly more accurate than those for the L_g waves. Thus, in spite of the high L_g/P ratios, the P wave has proved more useful for signal detection and for azimuth estimation than L_g, within the restraints of the present investigation.

The limitations of this study have not permitted the conclusion of the research. The optimum frequency band, the optimum signal flag, and the most useful combination of P and L_g information have not been determined. Two additional detection criteria have suggested themselves, during this work.

One is the observed stability of orientation, over several time windows, of the elongated particle-motion envelope, both in the P-wave portion of the record and in the L_g portion. The other is the observed ninety degree rotation of the envelope as the P-wave passes and the L_g wavetrain arrives. These items demand further study.

Finally, it appears from the research carried out thus far, that the principal utility of particle-motion processing lies not in signal detection, where the simple power detector is so successful, but in azimuth and distance determination. Of the missed signals in the P-wave detection trials discussed earlier, the P-wave processor estimated the back azimuth of half of them to within 5 degrees of their true back azimuth, even though it did not "detect" them. One of these signals was not visible even to the analyst. Moreover, the elongation of the figure traced by the reference particle has not been fully exploited in this study. The orientation of the elongation, measured in 3 dimensions and not just in the horizontal plane, will yield not only azimuth but emergence angle as well which indicates the source distance, and thus fixes location. The time between P and L_g, measured from the power rise at the signal onset down to the point where the particle-motion orientation rotates 90 degrees, also yields a distance estimate. Particle motion processing can also be exploited simply for picking phases. All of this potential must be addressed in future research.

E. Smart
H. Sproules

IMPROVED LOCATION TECHNIQUES WITH REGIONAL PHASES

A. Results of Location Experiments Using P_n Arrivals Using HYLO Methods

Since regional phase travel time curves depend on the details of crust-upper mantle structures it is important to evaluate the possibility of improving locations by using existing knowledge of the crust and upper mantle.

The evaluation of location accuracies using P_n and P_g arrivals with various regional and local crustal models in the Western United States (WUS) has shown that (Chang and Racine, 1980) the Herrin Model is an overall good average model for the crustal structure in the WUS. In that study varying crustal model for each source receiver path resulted in only small improvements in location errors, suggesting that the lateral heterogeneity in WUS is rather strong.

This result suggested that an alternate approach, called the HYLO method, reported by Herrin and Taggart (1962) might be a better way to allow for the lateral heterogeneity. In the HYLO method, the entire United States is subdivided by a grid of one degree squares and an estimated P_n velocity based on the crustal refraction data (Figure 22) is assigned to each square in the grid. The appropriate P_n travel time is then determined by ray tracing. In addition, in the present study the appropriate source station model from Chang and Racine (1980) is also assigned to each source-to-station path to allow for variations in crustal thickness at source or receiver.

The location accuracy of the modified HYLO method was tested with the same 12 nuclear explosions used by Chang and Racine. Location errors were compared to those obtained with the standard Herrin model, using P_n only, and P_n and P_g.

Comparison of location errors shown in Table IV shows the HYLO method is the worst of three methods. There are several possible explanations for this poor result. First, the P_n velocities assigned from interpolating the published contour lines may not be adequate. Second, the assigned crustal models may not be adequate. A new try should be made with separate models for source and receivers.

A. C. Chang
H. Sproules
J. A. Burnetti

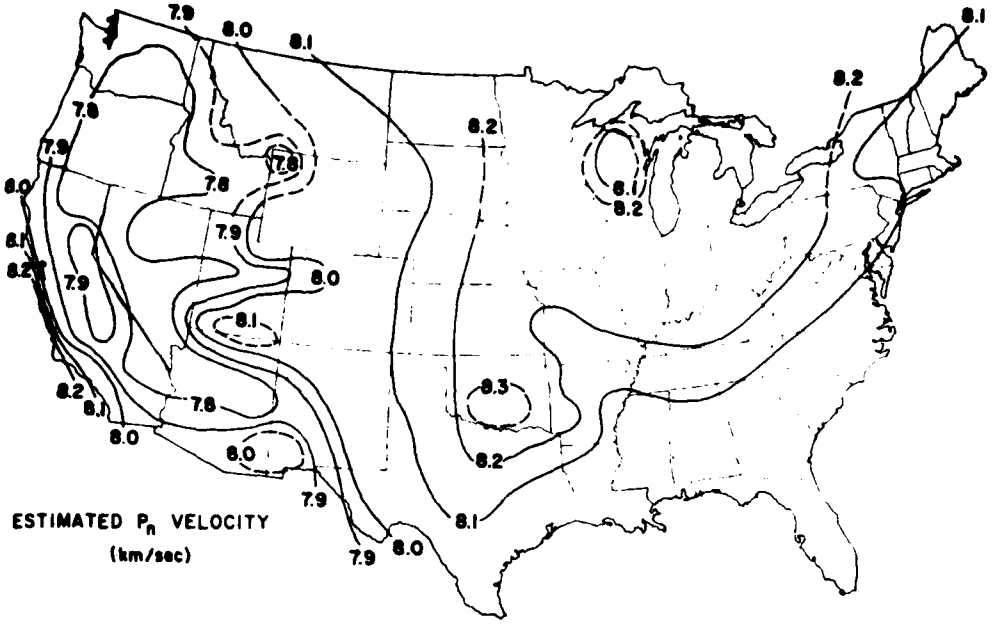

Figure 22. Estimated P_n velocity in the United States, based on data from deep seismic soundings, underground nuclear explosions, and earthquakes (compiled by E. Herrin and J. Taggart).

TABLE IV

COMPARISON OF LOCATION ERRORS

HYLO METHOD

	HERRIN Pn only		HERRIN(Pn + Pg)				HYLO			
	DEPTH REST		DEPTH REST		DEPTH FREE		DEPTH REST		DEPTH FREE	
	LOC E	OT E	LOC E*	OT E#	LOC E	OT E	LOC E	OT E	LOC E	OT E
Faultless	18.3	1.5	15.04	1.3	15.04	1.4	12.32	0.2	12.32	-1.8
Rulison	7.3	0.5	1.58	0.3	1.58	-0.1	3.63	1.3	3.72	1.0
Passaic	N/A	N/A	4.08	-0.4	4.08	-0.4	11.17	0.8	11.17	0.8
Rockville Dam	5.1	1.5	5.18	1.3	5.18	1.3	5.59	0.6	5.59	-0.4
Dormouse	N/A	N/A	9.09	-0.2	9.09	0.2	10.47	-0.8	10.47	-1.4
Klickitat	7.0	0.4	6.53	0.0	6.53	0.0	9.56	-0.5	9.64	0.6
Bandicoot	12.9	0.7	1.01	0.8	1.34	0.6	7.09	-0.6	7.09	-1.8
Shoal	5.9	0	5.18	0.1	5.18	4.1*	11.26	-0.7	11.26	0
Merrimac	10.3	0.3	9.58	0.2	9.58	1.0	10.99	-0.2	10.89	4.7
Gasbuggy	5.2	0.6	11.43	0.4	11.43	0.4	5.60	1.1	5.81	0.4
Piledriver	4.0	0.3	12.98	-0.4	12.98	1.2	24.54	-0.4	24.54	0.9
Roanoke	8.3	0.4	8.15	0.4	8.24	1.5	2.68	-0.6	3.68	0.4
Average	8.4		7.49		7.52		9.68		9.68	

* LOC E: Error of location vector, in km

\# OT E: Error of origin time estimates, $T_{est} - T_{true}$, in sec.

B. Results of Successive Locations Method

Conventional methods for calculating seismic hypocenter locations do not adequately compensate for the Earth's heterogeneity. Traditionally, the effect of the heterogeneous Earth in locating events has been corrected by master event techniques. Last year, Chang et al (1980) introduced two approaches to correct for structures at the source and station regions, and also to balance the effect of uneven distribution of seismic stations. These two methods resulted in improving location errors using teleseismic P arrivals. A similar approach to location using regional phases by Chang and Racine (1980) showed that location errors do not improve unless many local crustal models are utilized. The result reflects the fact that the Earth's heterogeneity is predominantly in the crust and upper mantle. A subsequent attempt to compute an average P_n velocity for each source-to-station path, called the HYLO method introduced by Herrin and Taggart (1962), resulted in no improvement in location errors. Although the complex nature of the P_n velocity variations in Nevada-Utah-Arizona area is well known (Figure 22), our experiments showed that the crust is far more complex and it is not adequate to use crustal models or use average P_n velocities computed from the published data.

A composite travel time chart (Figure 23) of 7 Nevada Test Sites (NTS) explosions in the test data base shows that both P_n and P_g are linear; therefore, it is possible to compute average P_n and P_g velocities for the NTS area. However, subsequent individual travel time charts show P_n velocities are slightly different from event to event. Figures 24 to 26 show some typical charts for NTS events. This indicates that an average velocity may not work as well as an individual velocity estimated for the individual event, particularly in the area as complex as NTS.

The successive locations method uses the Herrin crustal model to compute a preliminary location. Then the program computes P_n and P_g velocities using the obtained preliminary location. These estimated P_n and P_g will be used to locate the event again. This successive approximation cycle can be repeated.

At least three stations are needed to determine the velocity, but the reliability of the estimated velocity depends strongly on the number of inputs.

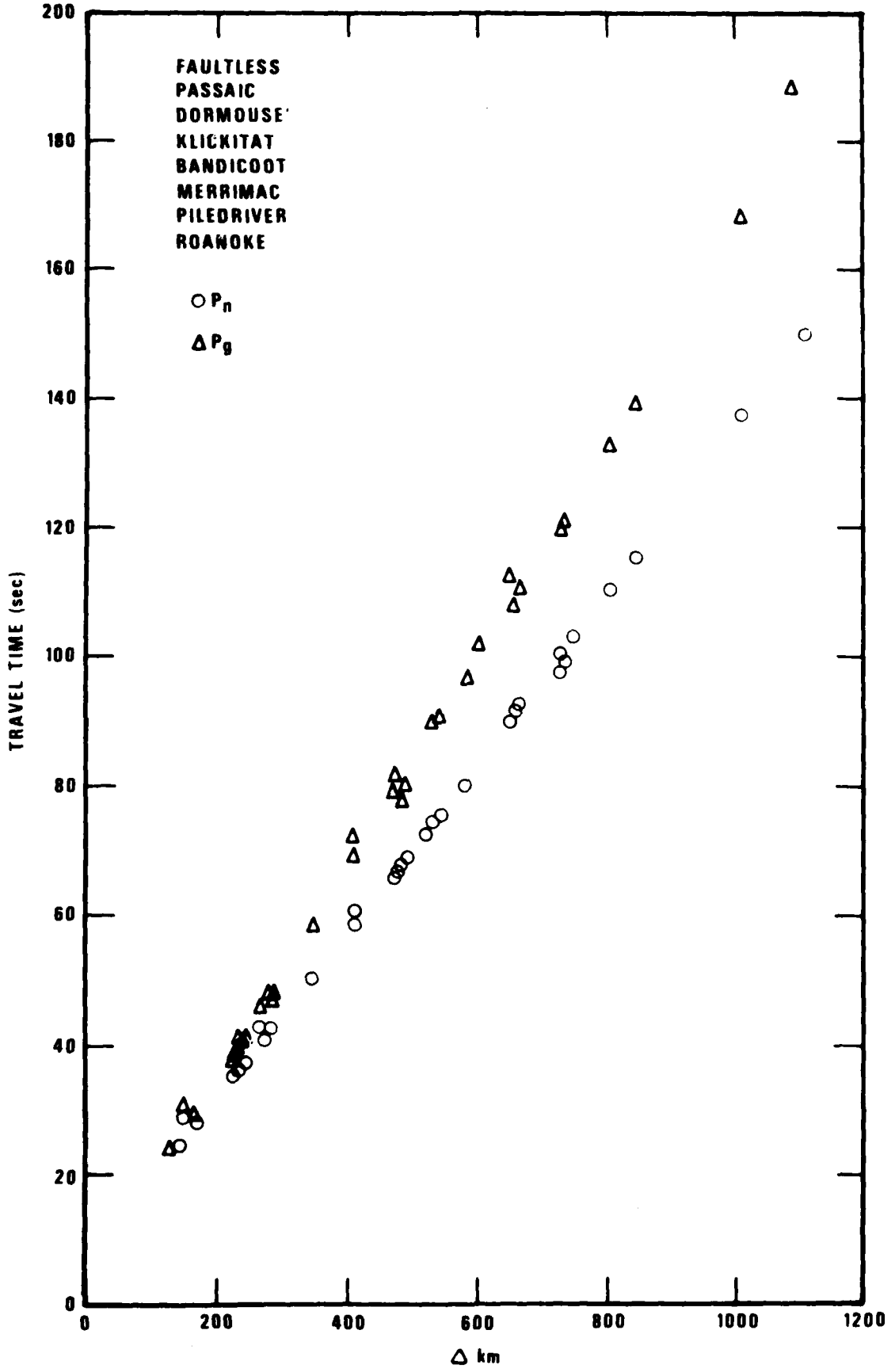

Figure 23. Composite travel time curves of P_n and P_g compiled from seven Nevada Test Site data.

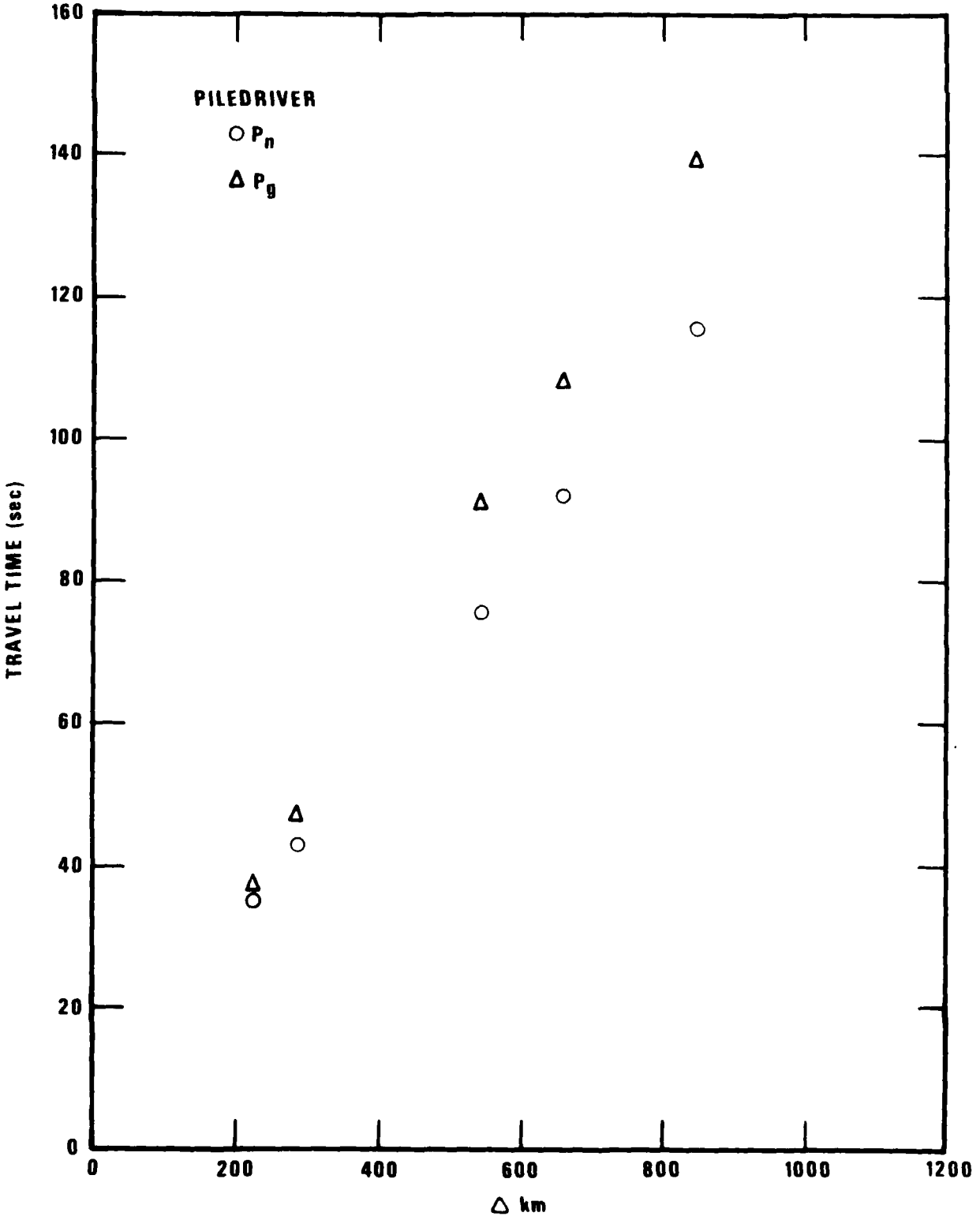

Figure 24. Travel time curves of P_n and P_g for PILEDRIVER event.

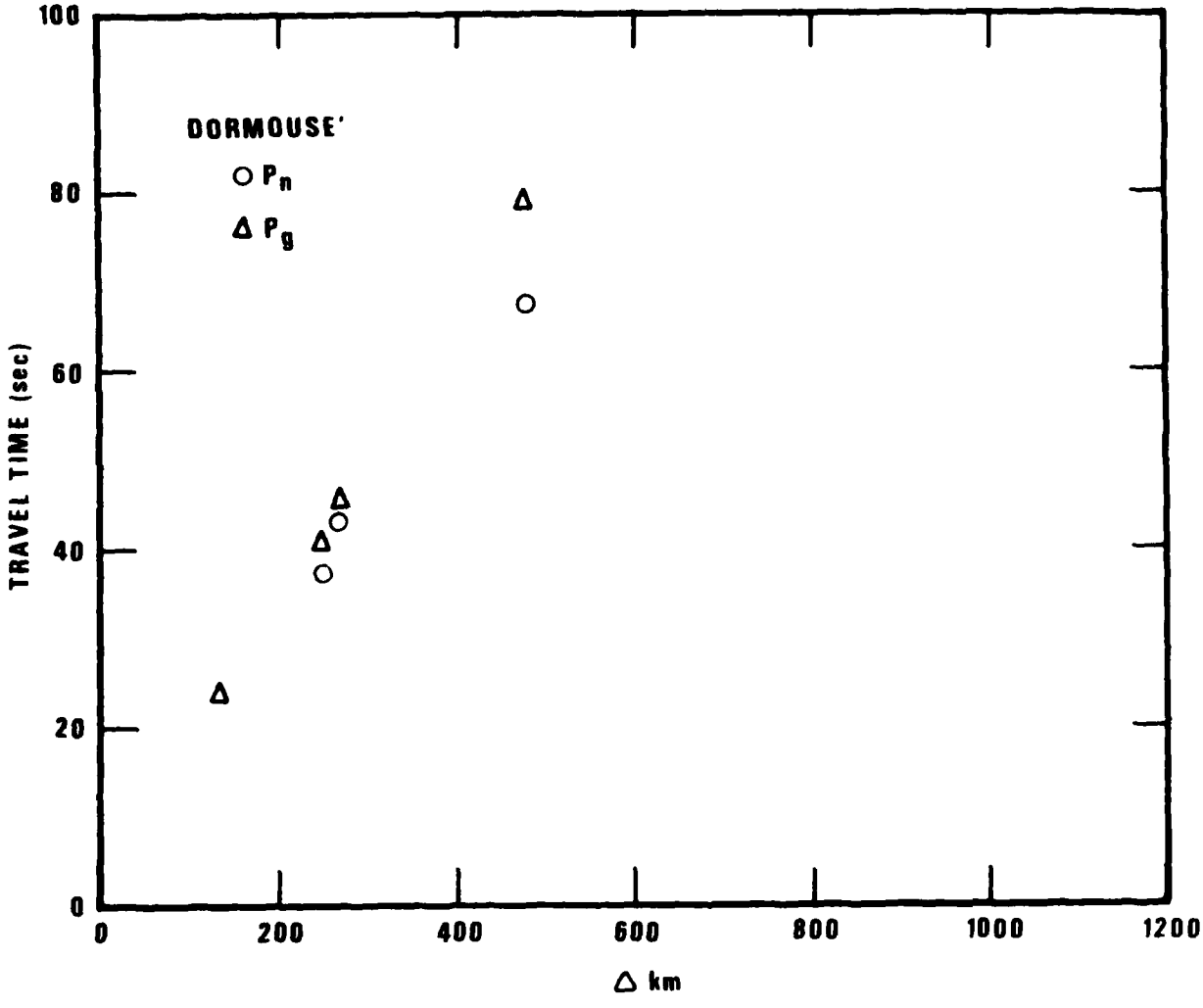

Figure 25. Travel time curves of P_n and P_g for DORMOUSE prime event.

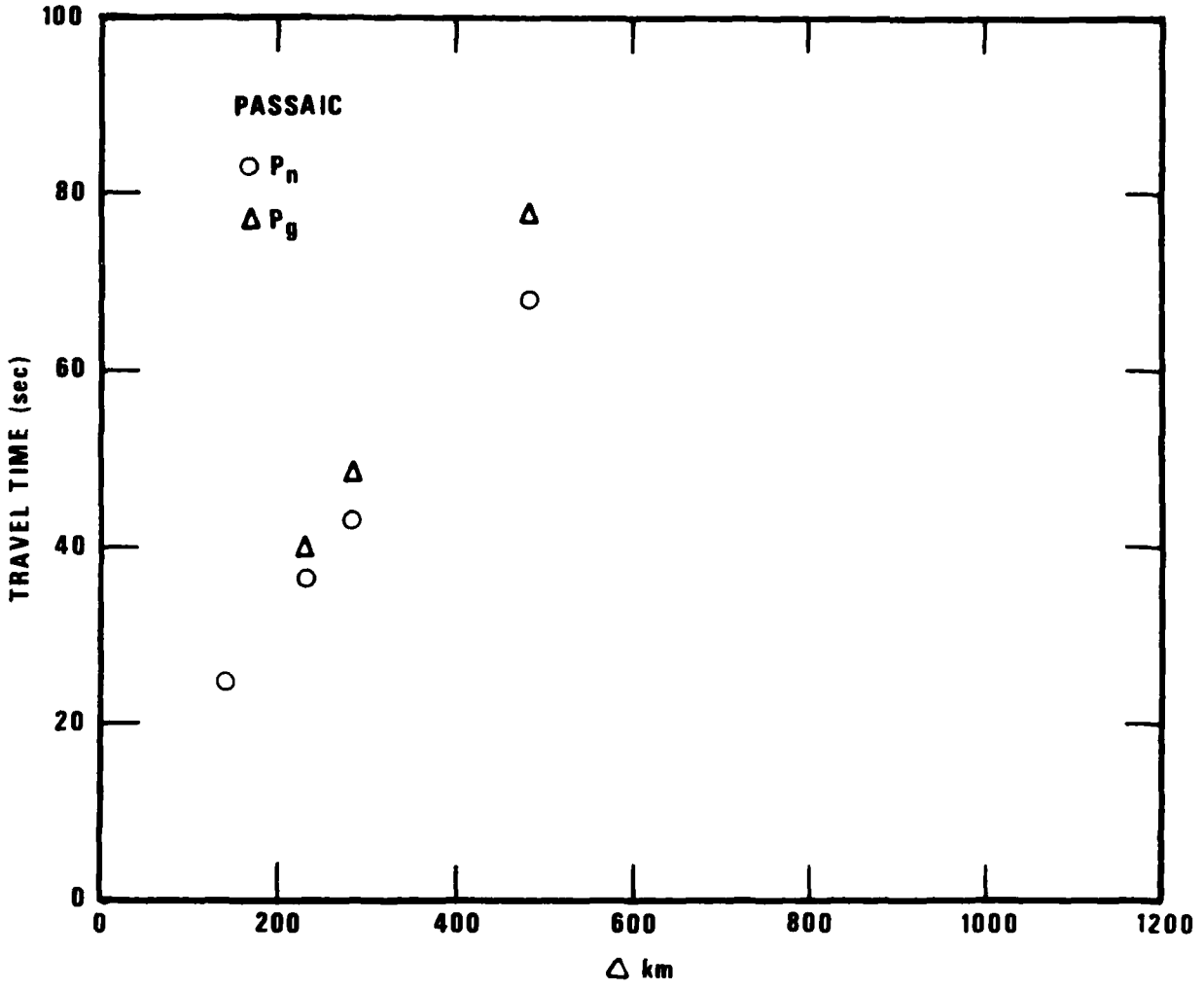

Figure 26. Travel time curves of P_n and P_g for PASSAIC event.

Furthermore, input stations with travel time residuals greater than 2.0 seconds are excluded in the velocity determination, because a station with a large error may significantly alter the estimated velocity. Standard errors are also estimated and they replace the built-in standard error values for each phase. Standard errors are used to weight inversely the signal phase in the location process. It was found that the ratio of P_n and P_g standard errors are near optimum at 1.0 to 3.0 as in the built-in ratio.

Table V shows the results in terms of location error vectors and origin time errors. Substantial improvements in location errors can be seen. Origin time errors and depth estimate errors are only as good as those using the Herrin travel time tables.

Romney et al (1962) demonstrated that there are clearly two distinct P_n velocities toward the East and toward the Northwest of the GNOME location. The location error of GNOME is 7.3 km with Herrin and 7.6 km with the successive location method. To account for two clearly different crusts, an option to estimate two sets of P_g and P_n velocities was created and tested. Using this dual successive determinations method the GNOME location error was reduced from 7.0 km to 5.4 km.

A. C. Chang
J. A. Burnetti

TABLE V

COMPARISON OF LOCATION ERRORS

SUCCESSIVE LOCATIONS METHODS

DEPTH FREE

	HERRIN			SUCCESSIVE LOCATIONS		
	LOC E[1].	OT. E[2].	DEPTH[3]	LOC. E.	OT. E.	DEPTH
Faultless	15.04	1.4	0.0	3.96	1.0	3.6
Rulison	1.58	0.0	0.0	3.39	2.6	0.0
Passaic	4.08	-0.2	0.0	2.14	-0.6	0.0
Rockville Dam	5.18	1.5	0.0	2.07	3.9	13.0
Dormouse Prime	9.09	0.2	0.0	9.87	0.7	4.3
Klickitat	6.53	0.1	0.0	2.78	0.7	8.1
Bandicoot	1.24	0.6	7.8	4.58	0.0	0.0
Shoal*	5.18	0.0	0.0	2.34	-0.9	0.0
Merrimac	9.58	0.3	0.0	5.16	0.2	15.9
Gasbuggy	11.43	0.6	0.0	10.04	2.0	0.0
Piledriver	12.98	0.0	0.0	1.66	-0.1	8.9
Roanoke	8.24	1.3	7.9	4.20	1.1	28.1
Average	7.52			4.35		

* Depth restricted

1. LOC. E.: Error of location vectors in km
2. OT. E.: Error of origin time estimates, $T_{est} - T_{true}$, in sec
3. when depth is zero, the depth is restricted to 0 km

C. Improved Location With Regional Phases

Method of Simultaneous Inversions

The standard technique of seismic event location involves assuming a trial value of the hypocenter and origin time, calculating predicted arrival times at a set of stations for signals originating at the trial hypocenter, and expanding the arrival time residual $\delta t = t_{observed} - t_{calculated}$ according to

$$\delta t = \frac{\partial t}{\partial T} dT + \frac{\partial t}{\partial x} dx + \frac{\partial t}{\partial y} dy + \frac{\partial t}{\partial h} dh,$$

and then adding the corrections dT, dx, dy, and dh to the assumed values of the origin time, east, north, and depth coordinates. In order to evaluate this equation for each residual δt, $\partial t/\partial T$ is set equal to unity at all stations and the other three partial derivatives are calculated by differentiating the travel-time curve for the signal in question (P, P_n, or P_g) at the proper epicenter to station distance Δ. In order to perform this differentiation, it is necessary to know accurately the values of the travel-time. In particular, for P_n and P_g the travel-time curves are known to be of the form

$$t_{P_n} = T + a_{P_n}(h) + b_{P_n} \Delta$$

where the coefficients a and b may be calculated from the assumed values of the thickness and the P-wave velocity for each layer of the crust in a laterally homogeneous earth model. The HYLO method consists of using locally measured, accurate values of the thicknesses and velocities for two-layer models in various regions of the earth in order to more accurately estimate the coefficients a and b and hence the partial derivatives $\partial t/\partial \Delta$ and $\partial t/\partial h$. The method of successive determinations assumes the thicknesses of the crustal layers to be known, but it determines the velocities (and hence the parameters b_{P_n} and b_{P_n}) by iteration. We describe herein a third method for differentiating the travel-time curves, one which assumes the coefficients a and b to be unknown parameters which are to be determined along with the hypocentral coordinates, T, x, y, and h. For n_1 observations of teleseismic P, n_2 observations of P_n, and n_3 observations of P_g, this method results in n_1 equations for arrival time residuals having the form described previously, n_2 equations of the form

$$\delta t = \frac{\partial t}{\partial T} dT + \frac{\partial t}{\partial x} dx + \frac{\partial t}{\partial y} dy + \frac{\partial t}{\partial a_{P_n}} da_{P_n} + \frac{\partial t}{\partial b_{P_n}},$$

and n_3 equations of a similar form involving a_{P_g} and b_{P_g}. The partial derivatives in these equations may be evaluated in a straightforward manner from the linear equations for the P_n and P_g travel times. The travel times for the regional phases are no longer explicitly depth-dependent, since all depth dependence is absorbed within the independent parameters a_{P_n} and a_{P_g}. Without teleseismic data, it is impossible to solve for the depth. Using the determined values of b_{P_g} and b_{P_n} however, one may find the P-wave crustal velocities and, if one assumes the thickness to be known, one may then solve for the depth using the values found for a_{P_n} and a_{P_g}. As can be seen from the linear equation for the P_n and P_g travel times, it is impossible to separate the origin time from a_{P_n} or a_{P_g}, so the origin time can be determined only if there are teleseismic measurements or if there are both P_n and P_g measurements.

In order to implement the method of simultaneous inversions, the standard location program LOCATION has been rewritten to solve for eight, rather than four, unknowns. Preliminary testing of the revised program shows it to be working satisfactorily. A detailed evaluation of the program is currently underway, using the same data base which was used for the method of successive determinations.

The coefficients a_{P_n}, b_{P_n}, a_{P_g} and b_{P_g} are the same for all events with epicenters close to each other. They may thus be determined more accurately if data from several nearby events are inverted simultaneously, a process known as joint epicenter determination (JED). The use of n epicenters results in a system of equations in 4n+4 unknowns. After the evaluation of the current version of the method of simultaneous inversions is completed, the method will be expanded to encompass the use of JED. The rewriting of program LOC was carried out in such a manner as to facilitate this extension, and the programming, testing, and evaluation of the method is expected to be completed by mid-June.

D. W. Rivers
A. C. Chang
J. A. Burnetti

D. Location with Regional Data

The traditional determination of hypocenters and origin times of seismic events involves finding the best values of the coordinates (latitude, longitude, depth, origin time) such that at a network of detecting stations the signal arrival time differences $\delta t = t_{observed} - t_{calculated}$ are minimized in a least-squares sense. In order to carry out the location, it is necessary to have measured arrival times at four or more stations in order that each of the four coordinates of the hypocenter can be determined uniquely. An accurate location, i.e., one for which the "error ellipsoid" formed by the confidence limits surrounding the calculated hypocenter is small, would obviously require several more than four measurements of arrival time. In practice, this requirement may be difficult to meet. One case in which it may not be met is that of a weak event for which the P-wave signal cannot be observed at teleseismic distances. Unless the area around the epicenter is densely populated by seismographic stations, it is unlikely that enough detections will be reported by stations at only regional distances to permit an accurate determination to be carried out. Another case in which the location may suffer from an insufficient number of arrival time measurements is that rather common instance in which, within some given time interval, several stations in a network have measured arrival times for P-waves, but the signals are from two or more different events (including local ones), and it is impossible to associate unambiguously each signal with the appropriate event.

These shortcomings of conventional location may be circumvented, or at least alleviated, by the use of more information than just the arrival time measurements. Smart (1977) has developed a surface-wave processor which enables three-component data to be inverted to yield the back azimuth of the epicenter at the detecting station. The back-azimuth measurements made by this processor are an excellent supplement to the arrival-time data. Even if no teleseismic measurements are available for an event, the surface-wave processor may still be used since, for regional events, the amplitude of L_g is comparable to that of P. In the case in which the P-wave detections cannot be associated unambiguously with a particular event, measurement of the back azimuth will in many cases resolve the ambiguity. In particular, arrival time and back azimuth measurements at only two stations would be sufficient to determine the hypocenter. Although this determination would

be crude, it should serve as an adequate trial value to permit the proper association of other signals with it. Back azimuth measurements are thus useful for event location, and we therefore have revised our standard location program LOCATION to use azimuth as well as arrival time data.

In the revised version of LOCATION, an initial trial value of the hypocenter and origin time is used to calculate the predicted signal arrival time and back azimuth at each station in a given network. Residuals are calculated by subtracting the predicted values from the observed values, and these residuals are then expressed in the form of a Taylor series about the trial coordinates. For a data base consisting of m arrival time measurements and n back-azimuth measurements, this process results in m equations of the form

$$\delta t = dT + \frac{\partial t}{\partial x} dx + \frac{\partial t}{\partial y} dy + \frac{\partial t}{\partial h} dh$$

and n equations of the form

$$\delta \zeta = \frac{\partial \zeta}{\partial x} dx + \frac{\partial \zeta}{\partial y} dy$$

where δt and $\delta \zeta$ are the arrival time and back azimuth residuals and dT, dx, dy, and dh are the corrections which are to be added to the trial value of the origin time, east, north, and depth coordinates. The partial derivatives in the arrival time equation may be calculated in the usual manner from travel-time curves, and those in the back azimuth equation may be determined by a straightforward solution for the appropriate spherical triangles. The resulting system of m+n equations may then be solved for the four unknowns, dT, dx, dy, and dh; these values are then added to the assumed hypocentral coordinates, yielding an improved location. This location is then used as a new trial value, and the process may be repeated through several iterations until the location converges. In practice, every residual δt ought to be weighted by the standard deviation of the appropriate arrival time measurement (e.g., 0.2 sec for P, 1.0 sec for P_n, 3.0 sec for P_g, etc.) and every residual $\delta \zeta$ ought to be weighted by the standard deviation of a back azimuth measurement, which Smart (1977) finds to be 7 degrees. Since the intersection of circles of radius $t \pm 1.0$ sec around each station comprises a much smaller area than does the intersection of sectors of angle $\zeta + 7$ degrees from each station, it is seen that the use of back azimuth data will offer very little improvement in the location beyond that which would be obtained by the use of several measurements of only the arrival time. Nevertheless, the back

azimuth data will be helpful when few arrival times were measured; in fact, the epicenter, but not the depth or origin time, may be calculated (crudely) from two back azimuth measurements alone. It may thus be possible to use this technique for locating "lonesome L_g" events.

The writing and debugging of the revised LOCATION program have been completed. The program was tested with azimuth inputs shown in Smart (1977) for SALMON and GNOME. Location errors are 417.4 km for SALMON and 202.3 km for GNOME. This result is approximately the same as the location errors found by Smart.

D. W. Rivers
A. C. Chang
J. A. Burnetti

EVASION

By detailed studies of explosions detonated in salt in the USSR we hope to better understand their source mechanism. This knowledge will make it possible to evaluate possibilities for evasion by decoupling in the USSR. For example, if the SALMON RDP is a satisfactory fit to the data then one might more reasonably use decoupling values and RDP's from STERLING in analyses of Soviet evasion.

One of the principal tools which we plan to use for investigation of the Soviet shots is the maximum likelihood estimator developed by Shumway and Blandford (1977). To check out its application to salt shots we have applied it to the initial P data recorded from the event SALMON. Figure 27 shows the likelihood contoured as a function of delay and amplitude of the secondary arrival. The source spectra used was that for SALMON, see e.g. Blandford and Woolson (1979), and the t* values were computed from the study of Der and McElfresh (1976).

The station plots are arranged in three profiles to the Northeast, North, and Northwest. We see that at all azimuths a pP echo with a delay of 0.55 ± 0.02 seconds and a reflection coefficient of approximately -0.4. The confidence intervals on arrival time are the population standard deviation of times determined at the 16 stations. Only at station WFMN does the reflection appear to be absent.

We see that there is also a multipath arrival with amplitude approximately +0.4 and arrival times ranging from 0.1 to 0.45 seconds with a mean and population standard deviation of 0.38 ± .08.

In addition, we occasionally see a negative amplitude arrival at small delays. This is especially prominent at the four closest stations on the North profile. We interpret this as a reflection from the interface between the top of the salt dome and the overlying sediments. This could account for its erratic appearance since the salt-sediment interface is doubtless more variable as a function of azimuth and angle to the vertical than is the free surface. One can be fairly sure that this is not just an artifact of the data processing because of the fact that Shumway and Blandford (1977) found no such reflections in the analysis of nine other events. Such a reflection would not have been expected from those events since they have no internal interfaces comparable in impedance to the salt-sediments interface.

At the top of Figure 27 is a calculation performed on the average of all 16 spectra, averaged after the effects of t* had been taken out by dividing by $\exp(-\omega t^*/2)$. We see that the main pP and the multipath arrival can still be seen.

The success of this approach as applied to SALMON suggests that the SALMON RDP is appropriate to SALMON as observed teleseismically. When moderate variations of the SALMON RDP are tried, pP cannot be detected with this approach. Thus the success of this method shows that the SALMON RDP is appropriate for the event.

In the lower left-hand corner of Figure 27 we see the same procedure, using the SALMON RDP and an independently determined t*, to analyze an April 25, 1975 shot from Azgir as recorded at NORSAR.

R. R. Blandford

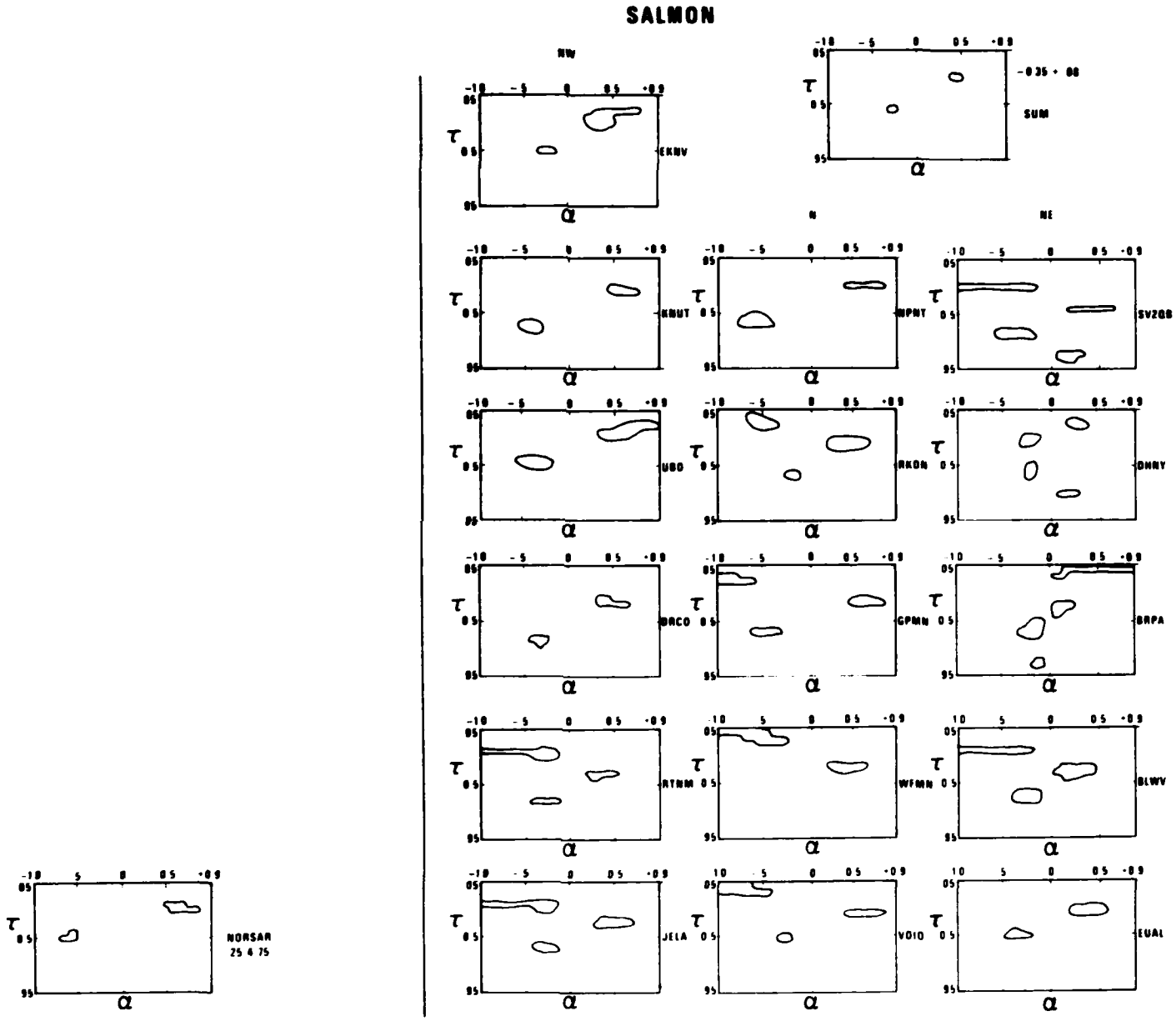

Figure 27. Contours of likelihood as a function of pP reflection coefficient, α, and delay, τ, for SALMON along three LRSM profiles. Also shown are the likelihood for an average spectrum where the average was computed after correction for individual t* values and the likelihood for an Azgir event recorded at NORSAR.

SUMMARY

The main findings of the research reported can be summarized as follows:

- The short-period surface wave L_g has been modeled by means of synthetic seismograms in order to determine the effects on the observed waveforms of propagation-path structure and to evaluate the feasibility of using L_g as a depth discriminant for shallow events.

- Amplitudes of regional phases P_n, P_g and L_g are significantly amplified by sediments. This affects yield estimation from regional phases, as well as discrimination.

- Envelope shapes of L_g wavetrains are also changed by sediments and this may influence any attempt to determine source depth from L_g.

- Phase velocities of L_g across small arrays are potentially useful as depth discriminants.

- Besides near surface sediments, scattering and local near-surface attenuation are also critical factors affecting regional phase characteristics.

- Analysis of Soviet data on amplitude-distance relationships of regional phases has been carried out to understand the effects of frequency and propagation path. The two largest-amplitude phases, L_g and P_g, show strong directional effects and Q increasing with frequency.

- An attempt was made to devise a regional event detector using the Smart processor. Signal and noise spectra were analyzed to determine differences in spectral shape. Good back-azimuths were obtained using the coherent fundamental-mode processor on the L_g phases, however, no reliable noise/signal discrimination statistic could be found. A new processor was developed, which used only the incoherent Love component of the signal. This processor gave excellent back-azimuths for both the L_g and P waves of the event. The oblateness of the motion, i.e., the ratio of the major axis to the minor axis of the envelope of particle motion, is a reliable detector but not necessarily better than a power detector.

- The test results of Herrin and Taggart's HYLO method were about 9.5 km in average errors. The failure to improve location accuracies may have been caused by the complexity of the WUS area. In the second subtask, the successive location methods showed an average location error of about

4.3 km. This result was very encouraging.

- A technique has been developed which performs event location while treating the slopes and intercepts of the (linear) P_n and P_g travel time curves as unknowns, thereby enabling an epicenter to be determined without reference to any *a priori* local earth model.

- The program modification to accept azimuth inputs from Smart's detector has been completed and tested. A preliminary test shows the location with azimuths only is capable of giving epicenter estimates which are comparable with locations obtained by Smart using another network method.

- A method has been developed for increasing the amount of data available for use in event location by incorporating into the data base measurements of back-azimuth made by Smart's (1977) detector.

- The success of the application of the maximum-likelihood determination techniques of Shumway and Blandford (1977) to SALMON and to an Azgir event of April 25, 1975, suggests that the latter events RDP may be adequately modeled by the SALMON RDP.

ACKNOWLEDGEMENT

We gratefully acknowledge useful comments by Dr. Shelton Alexander on the work. Ms. Anne O'Donnell helped in the preparation of some of the figures.

This work was supported by the Advanced Projects Agency of the U. S. Department of Defense under contract F080606-79-C-0007.

REFERENCES

Abo-Zeno, A. (1979). Dispersion function computations for unlimited frequency values, Geophys. J., 58, 91-105.

Aki, K. (1969). Analysis of the seismic coda of local earthquakes as scattered waves, J. Geophys. Res., 74, 615.

Aki, K. and B. Chouet (1975). Origin of coda waves, source attenuation and scattering effects, J. Geophys. Res., 80, 3322.

Antonova, L. V., F. F. Aptikayev, R. I. Kurochkina, I. L. Nersesov, A. V. Nikolayev, A. I. Ruzaykin, E. N. Sedova, A. V. Sitnikov, F. S. Tregub, L. D. Fedorskaya and V. I. Khalturin (1978). Experiment Seismic Studies of the Earth's Interior, Institute of Physics of the Earth, USSR Academy of Sciences, Nauka, Moscow, 155 pages.

Barker, B. W., Z. A. Der and C. P. Mrazek (1980). The effect of crustal structure on the regional phases Pg and Lg at NTS, Studies of Seismic Wave Characteristics at Regional Distances, AL-80-1, Teledyne Geotech, Alexandria, Virginia.

Barley, B. J. (1978). On the use of seismometer arrays to locate sources of higher mode Rayleigh waves, AWRE, Blacknest, England.

Blandford, R. R. and J. R. Woolson (1979). Experimental spectral analysis of SALMON/STERLING decoupling, SDAC-TR-79-3, Teledyne Geotech, Alexandria, Virginia.

Chang, A. C. and J. Burnetti (1980). Results of successive location and Pn, Pg velocity determination methods, SDAC Semi-annual Report.

Chang, A. C. and D. P. J. Racine (1980). Evaluation of location accuracies using Pn and Pg arrivals, SDAC-TR-80- , in press.

Chang, A. C., R. H. Shumway, R. R. Blandford and B. W. Barker (1980). Two methods to improve location estimates - Preliminary results, in press.

Der, Z. A. and T. W. McElfresh (1976). Short-period P-wave attenuation along various paths in North America as determined from P-wave spectra of the SALMON nuclear explosion, Bull. Seism. Soc. Am., 66(5), 1609-1622.

Gupta, I. N., B. W. Barker, J. A. Burnetti and Z. A. Der (1980). A study of regional phases from earthquakes and explosions in Western Russia, Bull. Seism. Soc. Am., 70, 851-872.

Herrin, E. and J. Taggart (1962). Regional variations in Pn velocity and their effect on the location of epicenters, Bull. Seism. Soc. Am., 52, 1037-1076.

Herrin, E. (1969). Regional variations of P-wave velocity in the upper mantle beneath North America, The Earth's Crust and Upper Mantle, Geogphysical Monograph #13, AGU, 242-246.

Helmberger, D. and D. Harkrider (1980). AFOSR report.

Knopoff, L., F. Schwab and E. Kausel (1973). Interpretation of Lg, Geophys. J., 33, 389-404.

Knopoff, L., F. Schwab, K. Nakanishi and F. Chang (1974). Evaluation of Lg as a discriminant among different continental crustal structures, Geophys. J., 39, 41-70.

Molnar, P., I. L. Nersesov, A. I. Ruzaikin, and V. I. Khalturin (1976). Lg waves and their propagation of Central Asia, Collection of Articles on Soviet-US Investigations on Earthquake Prediction, Publishing House "Donish," Dushambe-Moscow (in Russian).

Nersesov, I. L. and R. G. Rautian (1964). Kinematics and dynamics of seismic waves to distances of 3500 km from the epicenter, Akad. Nauk. SSSR, Trudy Inst. Fiziki Zemli, 32(199), 63-87.

Noponen, I. and J. Burnetti (1980). Alaskan regional data analysis, Studies of Seismic Wave Characteristics at Regional Distances, AL-80-1, Teledyne Geotech, Alexandria, Virginia.

Nuttli, O. W. (1973). Seismic wave attenuation and magnitude relations for eastern North America, J. Geophys. Res., 78, 876-885.

Oliver, J. and M. Ewing (1957). Higher modes of continental Rayleigh waves, Bull. Seism. Soc. Am., 47, 187-204.

Press, F. and M. Ewing (1952). Two slow surface waves across North America, Bull. Seis. Soc. Am., 42, 219-228.

Press, F. (1964). Seismic wave attenuation in the crust, J. Geophys. Res., 69, 4417-4418.

Romney, C., B. G. Brooks, R. H. Mansfield, D. S. Carder, J. N. Jordan and D. W. Gordon (1962). Travel times and amplitudes of principal body phases recorded from GNOME, Bull. Seism. Soc. Am., 52, 1057-1074.

Ruzaikin, A. I., I. L. Nersesov, V. I. Khalturin, and P. Molnar (1977). Propagation of Lg and lateral variations in crustal structure in Asia, J. Geophys. Res., 82, 307-316.

Shishkevish, C. (1979). Propagation of Lg seismic waves in the Soviet Union, Report N-1014-ARPA, Rand Corporation, Sant Monica, California.

Shumway, R. H. and R. R. Blandford (1977). On detecting and estimating multiple arrivals from underground nuclear explosions, SDAC-TR-77-8, Teledyne Geotech, Alexandria, Virginia.

Smart, E. (1977). A 3-component single-station maximum likelihood signal processor, SDAC-TR-77-14, Teledyne Geotech, Alexandria, Virginia.

Stephens, C. and B. L. Isacks (1977). Toward an understanding of Sn: normal modes of Love waves in an oceanic structure, Bull. Seism Soc. Am., 67, 69-78.